Contrib Mineral Petrol (2002) 144: 365–382
DOI 10.1007/s00410-002-0403-4

ORIGINAL PAPER

Laurent Desmurs · Othmar Müntener
Gianreto Manatschal

Onset of magmatic accretion within a magma-poor rifted margin: a case study from the Platta ocean-continent transition, eastern Switzerland

Received: 24 January 2002 / Accepted: 25 July 2002 / Published online: 28 September 2002
© Springer-Verlag 2002

Abstract Exhumation of subcontinental mantle rocks and its exposure at the seafloor is known from different magma-poor passive continental margins. However, the transition from largely amagmatic passive rifting to seafloor spreading is still poorly documented. In this contribution we use MOR-type gabbroic and basaltic rocks to characterize the magmatism associated with the formation of an ancient ocean-continent transition preserved in the Platta nappe, eastern Switzerland. Gabbros form individual small intrusions into exhumed serpentinized subcontinental mantle rocks. Mineral and bulk-rock chemistry and simple modeling indicate that each gabbro body records different magmatic processes ranging from predominantly fractional crystallization to solidification without fractionation. Mg numbers and Ni contents of equilibrium olivine calculated from basalts and gabbros indicate that few mafic rocks are primary melts but most represent fractionated compositions ranging from T- to N-MORB. Whereas most mafic rocks may be explained by low to moderate degrees of melting of an N-MORB-type mantle, the source of some basalt is enriched in incompatible elements. This compositional variation seems to correlate with the spatial distribution of the mafic rocks within the ocean-continent transition whereby mafic rocks with T-MORB signatures occur close to the continental margin whereas N-MORB signatures are predominantly found oceanwards. As in an opening system time and space are closely linked, the chemical evolution of the mafic rocks along the ocean-continent transitions suggests continuous thinning of the subcontinental mantle and associated uplift of the underlying asthenosphere during the time between the crustal and the lithospheric breakup.

L. Desmurs
Department of Earth Sciences,
Federal Institute of Technology,
ETH-Zentrum, 8092 Zürich, Switzerland

O. Müntener (✉)
Institute de Géologie, Université de Neuchâtel,
Rue Emile Argand 11,
2007 Neuchâtel, Switzerland
E-mail: othmar.muentener@unine.ch
Tel.: +41-32-7182659
Fax: +41-32-7182601

G. Manatschal
CGS-EOST–UMR 7517 CNRS-ULP,
1 Rue Blessig,
67064 Strasbourg, France

Editorial responsibility: J. Hoefs

Introduction

In the Alps, ophiolites derived from the Mesozoic Liguria-Piedmont ocean consist predominantly of a serpentinized peridotite basement covered by deep-sea sediments, magmatic rocks being only subordinate. This stratigraphy, related to the exposure of mantle rocks on the seafloor, has been interpreted as formed either along a slow-spreading ridge (Lagabrielle and Lemoine 1997) or by tectonic exhumation of subcontinental mantle during earlier Jurassic rifting (Lemoine et al. 1987; Piccardo et al. 1990; Froitzheim and Manatschal 1996).

In either case, the formation of a slow spreading ridge is necessarily preceded by a period of rifting and, at some point, there must be a transition from (largely) amagmatic passive rifting to the formation of igneous crust and finally the establishment of a slow spreading system.

Geological studies on land and geophysical studies at sea show that, along so-called non-volcanic margins, an ocean-continent transition zone several tens of kilometer wide separates thinned continental crust from oceanic crust (e.g., Manatschal and Nievergelt 1997; Müntener and Hermann 2001; Whitmarsh et al. 2001). This zone consists predominantly of exhumed mantle rocks locally intruded and overlain by MOR-type mafic rocks. It is the purpose of this paper to provide constraints on the igneous accretion within this transition zone.

source: https://doi.org/10.7892/boris.87469 | downloaded: 19.4.2024

Based on field and geochemical evidence, it has been demonstrated that in the Alps, the serpentinite basement of the ocean-continent transition represents former subcontinental mantle (Piccardo et al. 1990; Trommsdorff et al. 1993; Rampone et al. 1995; Müntener and Hermann 1996) exhumed during rifting, leading to the opening of the Alpine Tethys (Müntener et al. 2000). This subcontinental mantle was intruded by gabbroic rocks and locally covered by basaltic volcanics showing MORB affinities. By analogy with results obtained from the Galicia bank and the Iberian margin (Boillot et al. 1987; Schärer et al. 1995; Charpentier at al. 1998; Cornen et al. 1999; Schärer et al. 2000), the gabbros are classically interpreted as pre-dating breakup of the continental crust (syn-rift gabbros; Rampone et al. 1998) whereas, according to this terminology, the basalts overlying exhumed mantle rocks necessarily belong to the post-rift sequence. However, as they overly tectonically exhumed subcontinental mantle, their extrusion pre-dates the breakup of the continental lithosphere, which corresponds to the emplacement of an oceanic spreading system.

The Totalp-Platta-Malenco ultramafic and mafic rocks in eastern Switzerland and northern Italy are, together with the overlying Austroalpine Err and Margna nappes, the relicts of a fossil ocean-continent transition (OCT) which can be reconstructed with some confidence (Manatschal and Nievergelt 1997; Müntener and Hermann 2001; Desmurs et al. 2001). In this contribution, we provide new mineralogical and chemical data on mafic rocks from the Platta nappe which demonstrate that these isolated bodies of MORB-type magmatic rocks record the initiation of magmatic accretion within the ocean-continent transition zone during a transitional stage between the crustal and lithospheric breakup of the continental lithosphere.

Regional geology

The Err and Platta nappes are part of a late Cretaceous west-directed thrust wedge which was probably associated with subduction along the eastern border of Adria (Froitzheim et al. 1996). In a later stage, this nappe stack was thrust 'en bloc' towards the north over the European units during the Tertiary (Froitzheim et al. 1996). The south-Pennine ophiolites of the Arosa zone, the Platta nappe and the Malenco complex lack a high-pressure metamorphic overprint associated elsewhere with the Tertiary subduction, and show only a general increase of Alpine metamorphism from deep burial diagenesis in the north (Arosa zone, Trommsdorff 1983; Ferreiro-Mählmann 1995) to epidote-amphibolite facies conditions in the south (Malenco complex, Trommsdorff and Evans 1974).

Together with the lower Austroalpine Err nappe, the Platta nappe preserves the remnants of a segment of the southeastern margin of the Liguria-Piedmont Ocean (Fig. 1). The Err nappe includes the relicts of the distal Adriatic margin and was thrust onto the Platta nappe during late Cretaceous times. It consists of a thinned continental crust, overlain by a number of extensional allochthons, slivers of continental crust and pre-rift sediments which were tectonically emplaced during the late-Middle Jurassic along an oceanward-dipping low-angle detachment system (Froitzheim and Eberli 1990; Froitzheim and Manatschal 1996; Manatschal and Nievergelt 1997). The Platta nappe, originally situated oceanwards of the Err nappe, represents the ocean-continent transition s.str. and exposes serpentinized peridotites, minor gabbroic rocks, basaltic volcanics and oceanic sediments. Far-traveled extensional allochthons, derived from the distal continental margin, were emplaced on the exhumed mantle rocks prior to the deposition of the basalts (Manatschal and Nievergelt 1997).

Palinspastic reconstructions (Manatschal and Nievergelt 1997; Desmurs et al. 2001) have shown that the Platta nappe consists of two large sheets of ultramafic rocks, an upper and originally continentalward one and a lower, originally oceanward one (Fig. 1b, c). The latter is covered by pillow lavas and basaltic flows and was locally intruded by Jurassic gabbros 161 ± 1 Ma ago (Schaltegger et al. 2002), which crystallized at shallow depth within an already serpentinized mantle (Desmurs et al. 2001). Both gabbros and basalts are derived from a similar mantle source, as demonstrated by their ϵNd values up to $+9$ determined on whole rocks and by the ϵHf up to $+15$ of the zircons of the gabbros (Schaltegger et al. 2002). The upper serpentinite unit is almost free of magmatic rocks, except for a few dolerite dykes and a single basaltic flow.

Gabbros

Field relationships

Within the Platta nappe, gabbros occur in two main areas in the lower serpentinite unit, near Fuorcla da Faller and in Val da Natons (Fig. 1b). In the Fuorcla da Faller area, an individual gabbro body, about 100 m across, largely preserves its internal magmatic relationships. This body shows a high diversity in composition, from primitive olivine-gabbro to highly differentiated Fe-Ti-P- gabbros and diorite, and it is characterized by a lack of layering and of systematic vertical changes (Fig. 2). The main part of the body ($\sim$90%) consists of Mg-gabbro (samples P4, MS13, MS15, MS9) with plagioclase and clinopyroxene as the main constituents. Locally, the gabbros are cut by or grade into high-temperature shear zones showing a marked decrease in grain size. The Mg-gabbro shows a diffuse contact with a Fe-gabbro (sample MS3, clinopyroxene-hastingsitic hornblende-Fe-Ti oxide-plagioclase, 5% of the outcrop). The Mg-gabbros may also

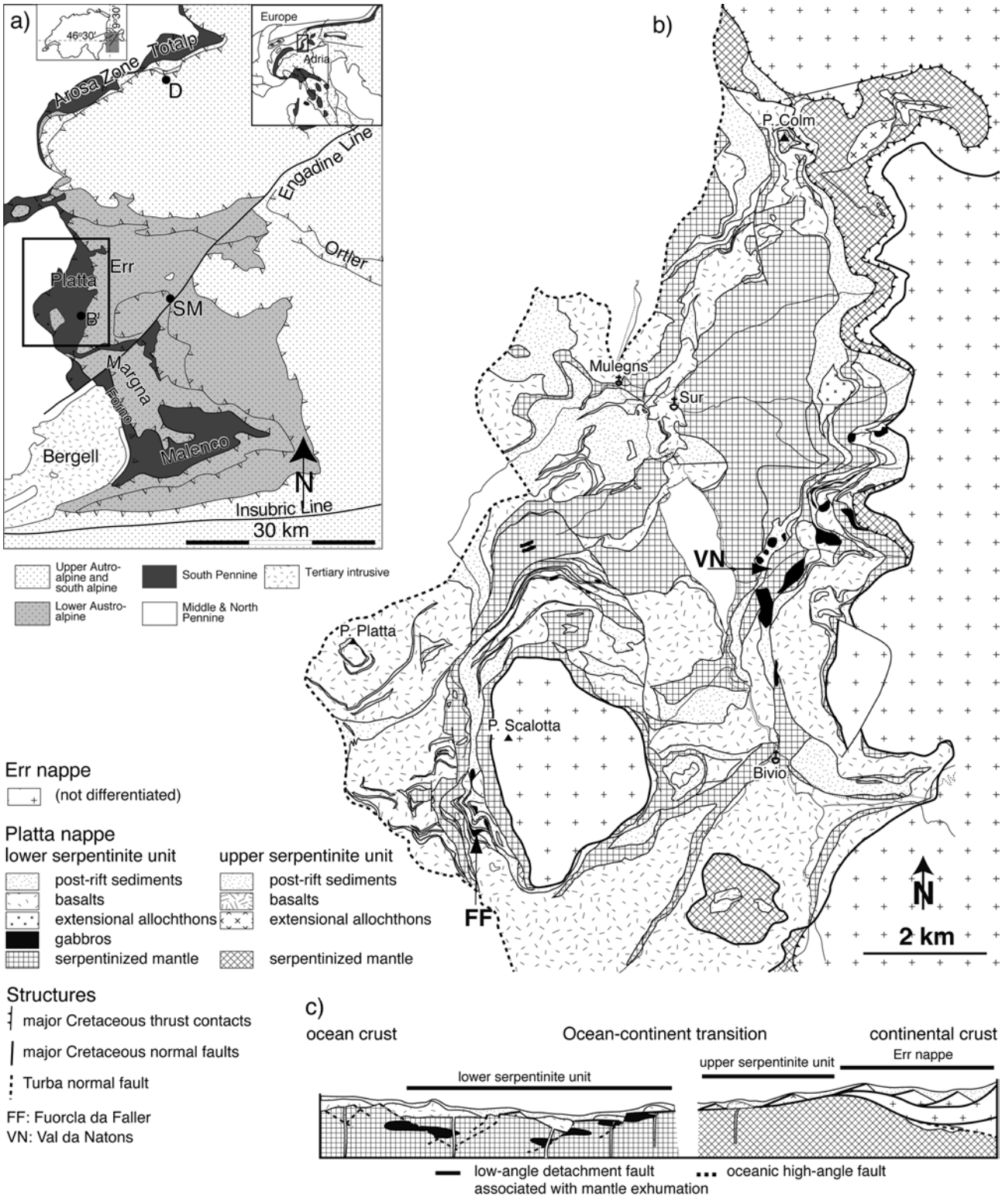

Fig. 1 **a** Simplified tectonic map and location of the study area. *B* Bivio, *D* Davos, *SM* St. Moritz (modified after Froitzheim et al. 1994). **b** Tectonic map, and **c** palinspastic profile of the Platta nappe (after Cornelius 1932, Dietrich 1969, and own mapping)

contain small pockets of Fe-gabbros but the opposite relationship is also observed. Both gabbro types are cut by a Fe-Ti-P-gabbro (sample P9, clinopyroxene-pargasitic hornblende-ilmenite-plagioclase-apatite-zircon). Pegmatitic diorite (sample MS10, pargasitic hornblende-plagioclase-clinopyroxene-quartz) occurs as patches or dykes which form boudins or folds within the Mg-gabbro, indicating syn-magmatic deformation. In some of these patches, Fe-Ti-P-gabbro and diorite occur together (Fig. 2). The gabbro body is locally cut by basaltic dykes

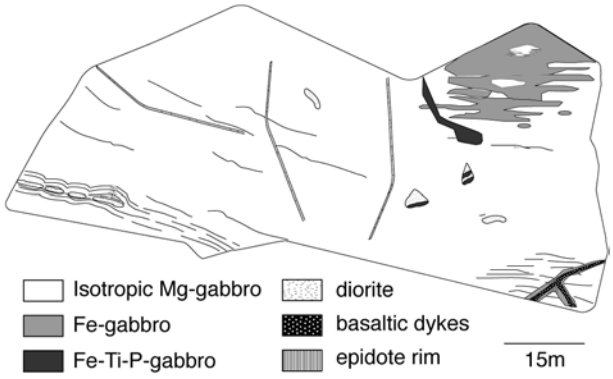

Fig. 2 Schematic sketch of the magmatic relationships observed in the Fuorcla da Faller gabbro. Mg-gabbros make up the main part of the body. They show large grain-size variations and are cut by discrete high-temperature shear zones. A more differentiated Fe-gabbro crystallized at the edge of the body and is interfingered with the Mg-gabbro. Both rock types are cut by a Fe-Ti-P-gabbro, which was also found in pockets at the center of the body together with diorite. The diorite is also present as dykes throughout the whole body but never exceeds 20 cm in thickness. Basaltic dykes cut across the gabbros and are characterized by a wide, epidote-rich rim and by chilled margins

with chilled margins indicating that emplacement of the dykes took place after cooling of the gabbro. The primary contact to the host rock, most likely serpentinite, is strongly overprinted by Alpine deformation, However, we assume that the sediments, serpentinite and gabbro observed in the field largely represent the primary association.

In Val da Natons, several gabbro outcrops (Fig. 1b) consist mainly of Mg-gabbro bodies, some tens of meters across, except for a much larger one (0.5 km long and 50 m thick) which shows the same diversity of rock types as the gabbros at Fuorcla da Faller. One of the small Mg-gabbros (sample NAG3) shows an increase in grain size from the rim to the core of the body; the other one is cut by a few small dykes of diorite (sample NAG9). Both show evidence for localized internal deformation under retrograde metamorphic conditions from amphibolite to greenschist facies. Locally, they are stratigraphically overlain by sedimentary and pillow breccias containing gabbro clasts, demonstrating their exhumation and exposure at the seafloor (Desmurs et al. 2001).

Petrography

The Mg-gabbros show euhedral plagioclase, sub- to anhedral clinopyroxene and in a few samples interstitial Ti-pargasite. In many places clinopyroxene and plagioclase show graphic intergrowth indicating cotectic crystallization of the two phases. Plagioclase is always altered to a fine-grained mixture of albite, chlorite, epidote, prehnite and pumpellyite. In the Mg-gabbros, Ti-pargasite occurs as interstitial grains between plagioclase

Table 1 Chemical composition of clinopyroxene of the Platta gabbros

Sample[a]	Mg-gabbro															
	P4		MS9		SC5				MS8		NAG9		MS13		NAG3	
	Core		Core		Core		Neoblast		Core		Core[b]		Core		Core	
SiO_2	51.12	0.44	51.33	0.86	50.31	0.89	49.45	0.96	51.03	0.77	53.50	0.78	51.16	0.94	50.33	0.35
TiO_2	0.65	0.05	1.14	0.31	1.33	0.28	1.66	0.15	0.97	0.39	0.28	0.15	0.86	0.26	0.94	0.11
Cr_2O_3	1.26	0.09	0.06	0.02	0.18	0.08	0.18	0.19	0.03	0.02	0.10	0.04	0.08	0.06	0.17	0.05
Al_2O_3	4.03	0.18	3.30	0.16	3.29	0.58	3.62	0.79	3.13	0.23	1.53	1.00	3.16	0.68	2.79	0.25
Fe_2O_3	1.85	0.39	2.24	1.33	2.36	0.55	2.58	0.30	3.02	1.09	1.03	0.52	1.48	0.84	2.45	0.56
FeO	1.79	0.39	5.11	0.90	5.39	0.70	6.09	1.31	5.16	0.48	3.78	0.45	5.97	1.07	3.60	0.48
MnO	0.08	0.04	0.20	0.03	0.17	0.05	0.20	0.05	0.23	0.09	0.14	0.02	0.21	0.05	0.16	0.02
MgO	16.41	0.25	14.84	0.60	14.95	0.63	14.41	0.78	15.30	0.60	15.98	0.47	15.31	0.50	15.49	0.17
CaO	21.99	0.41	21.46	0.48	21.65	0.50	21.47	0.18	20.85	1.06	23.41	1.69	20.60	1.52	22.32	0.24
Na_2O	0.69	0.09	0.56	0.07	0.54	0.10	0.60	0.11	0.54	0.09	0.48	0.20	0.56	0.16	0.46	0.05
K_2O	0.01	0.01	0.03	0.05	0.00	0.01	0.01	0.01	0.01	0.01	0.03	0.01	0.01	0.01	0.01	0.01
Total	99.89	0.59	100.26	0.80	100.20	0.61	100.30	0.92	100.28	0.62	100.27	0.54	99.41	0.65	98.73	0.48
Si	1.876	0.007	1.893	0.045	1.874	0.022	1.851	0.019	1.882	0.018	1.961	0.024	1.906	0.030	1.891	0.006
Ti	0.018	0.001	0.032	0.009	0.037	0.008	0.047	0.005	0.027	0.011	0.008	0.004	0.024	0.007	0.026	0.003
Cr	0.036	0.003	0.002	0.001	0.005	0.002	0.005	0.006	0.001	0.001	0.003	0.001	0.002	0.002	0.005	0.002
Al	0.174	0.008	0.144	0.007	0.144	0.025	0.159	0.033	0.136	0.011	0.066	0.043	0.139	0.030	0.124	0.011
Fe^{3+}	0.051	0.011	0.062	0.037	0.066	0.016	0.073	0.009	0.084	0.031	0.028	0.014	0.042	0.024	0.069	0.016
Fe^{2+}	0.055	0.012	0.158	0.029	0.168	0.023	0.191	0.044	0.159	0.015	0.116	0.014	0.186	0.033	0.113	0.015
Mn	0.002	0.001	0.006	0.001	0.005	0.002	0.006	0.002	0.007	0.003	0.004	0.000	0.007	0.001	0.005	0.001
Mg	0.897	0.013	0.815	0.027	0.830	0.030	0.804	0.032	0.841	0.033	0.873	0.025	0.850	0.027	0.868	0.011
Ca	0.865	0.015	0.848	0.014	0.864	0.018	0.861	0.015	0.824	0.040	0.919	0.065	0.822	0.060	0.899	0.010
Na	0.049	0.007	0.040	0.005	0.039	0.007	0.043	0.008	0.038	0.006	0.034	0.014	0.040	0.011	0.033	0.003
K	0.000	0.000	0.001	0.002	0.000	0.000	0.000	0.000	0.001	0.000	0.001	0.001	0.000	0.001	0.000	0.000
Mg#	0.895	0.005	0.788	0.003	0.780	0.024	0.753	0.040	0.776	0.018	0.858	0.011	0.789	0.011	0.826	0.007

[a]For each sample, the average composition is shown in the first column and the standard deviation (2σ) is shown in the second column of six oxygens. $Mg\# = Mg/(Fe^{3+} + Fe^{2+} + Mg)$

and/or clinopyroxene or may form rims around or patches within clinopyroxene grains. Fe-gabbros consist of anhedral to subhedral clinopyroxene and plagioclase with interstitial ilmenite. Ti-rich hornblende occurs mainly as rims around ilmenite or as interstitial grains between Fe-Ti-oxide and clinopyroxene. The Fe-Ti-P-gabbro is made of euhedral plagioclase and apatite, subhedral clinopyroxene, and interstitial pargasite and ilmenite; euhedral zircon also occurs in a few samples. The pegmatitic diorite contains large euhedral plagioclase crystals, large sub- to anhedral magnesian hornblende, quartz, large anhedral zircon, and rare and strongly altered clinopyroxene showing a symplectitic texture with Ti-pargasite. Clinopyroxene with a similar texture and mineralogy was found in the Mg-gabbro at the contact with the diorite, suggesting that the clinopyroxenes in the diorite are xenocrysts from the Mg-gabbro.

Internal deformation is observed in all gabbro bodies mostly as discrete, high-temperature shear zones related to the magmatic emplacement. The highest temperature deformation is recorded by a syn-magmatic foliation defined by small clinopyroxene, pargasite and apatite granoblasts showing typical triple-junction grain boundaries and no crystal-plastic deformation. Pargasite and ilmenite occur also as undeformed interstitial grains between the neoblasts, which has been interpreted as evidence for a late-magmatic stage of deformation (Desmurs et al. 2001).

In Val da Natons, retrograde mylonitic shear zones are also observed. The mylonitic foliation is defined by small neoblasts of actinolite and albite, or by albite, chlorite and rare biotite which crystallized between clasts of clinopyroxene. The recrystallization of albite and actinolite and the deformation of chlorite and biotite suggest that these shear zones were active under lower amphibolite to greenschist facies conditions. These shear zones were later affected by cataclastic deformation and intense veining during which epidote, chlorite and albite crystallized.

Mineral chemistry

Clinopyroxene

The augitic clinopyroxenes of the gabbros of the Platta nappe are characterized by low Al_2O_3 (<4.5 wt%) and Na_2O (<0.71 wt%) contents (Table 1) which are similar for the different gabbro types and are also similar to those of gabbros from the Ligurian Apennines (Tribuzio et al. 1999). However, the Mg# of these minerals continuously decreases from the Mg-gabbro (0.90–0.74) to the Fe-gabbro (0.71–0.68) and the highly differentiated Fe-Ti-P-gabbro (0.66–0.63). This decrease in Mg# correlates with an increase of MnO and a decrease of TiO_2, Al_2O_3 and Cr_2O_3 (Fig. 3). The composition of the clinopyroxene is generally homogeneous within single

								Fe-gabbro				Fe-Ti-P-gabbro					
		MSG2-2				MS10		MS3		NAG5		P9		NAG7			
Rim		Core		Core[b]		Core[b]		Core		Core		Core		Porphyroclast		Neoblast	
49.74	0.56	51.25	0.71	52.51	1.21	52.76	0.66	51.18	0.33	52.02	0.50	51.20	0.53	51.39	0.55	52.18	0.31
1.27	0.07	0.77	0.18	0.48	0.27	0.45	0.19	1.00	0.15	0.28	0.14	0.66	0.14	0.47	0.08	0.19	0.05
0.03	0.02	0.03	0.02	0.03	0.02	0.05	0.01	0.01	0.02	0.01	0.01	0.01	0.01	0.01	0.01	0.01	0.01
2.65	0.36	2.81	0.42	1.79	0.80	1.87	0.54	2.52	0.19	1.15	0.27	1.94	0.18	1.42	0.22	0.83	0.13
2.35	0.56	2.68	0.55	1.90	0.73	1.70	0.30	1.99	0.21	1.36	0.42	3.30	1.41	0.99	0.79	0.22	0.30
5.79	1.03	3.90	0.63	4.76	0.98	4.14	0.29	8.40	0.36	9.75	0.43	8.85	0.51	11.52	0.64	11.77	0.26
0.23	0.04	0.20	0.04	0.22	0.03	0.22	0.04	0.30	0.02	0.47	0.04	0.38	0.05	0.51	0.05	0.52	0.03
14.07	0.47	15.45	0.55	16.25	0.96	16.25	0.18	13.74	0.32	12.97	0.27	12.69	0.63	11.75	0.21	11.82	0.22
21.84	0.19	21.88	0.69	21.20	2.16	22.02	0.88	20.66	0.45	20.92	0.57	19.92	0.94	20.49	0.36	21.01	0.25
0.60	0.02	0.75	0.12	0.55	0.26	0.59	0.11	0.71	0.12	0.62	0.10	0.94	0.54	0.64	0.13	0.48	0.05
0.01	0.01	0.01	0.01	0.00	0.01	0.01	0.01	0.02	0.01	0.01	0.02	0.02	0.01	0.03	0.04	0.01	0.01
98.61	0.42	99.73	0.68	99.70	1.02	100.04	0.69	100.53	0.38	99.59	0.73	99.92	0.59	99.23	0.84	99.03	0.66
1.890	0.015	1.906	0.015	1.945	0.036	1.944	0.014	1.914	0.008	1.970	0.010	1.926	0.020	1.965	0.011	1.992	0.007
0.036	0.002	0.022	0.005	0.013	0.007	0.012	0.005	0.028	0.004	0.008	0.004	0.019	0.004	0.013	0.002	0.005	0.001
0.001	0.001	0.001	0.001	0.001	0.001	0.001	0.000	0.000	0.000	0.000	0.000	0.000	0.000	0.000	0.000	0.000	0.000
0.119	0.016	0.123	0.019	0.078	0.035	0.081	0.024	0.111	0.009	0.051	0.012	0.086	0.008	0.064	0.010	0.037	0.006
0.067	0.016	0.075	0.016	0.053	0.020	0.047	0.009	0.056	0.006	0.039	0.012	0.093	0.040	0.029	0.023	0.006	0.008
0.184	0.033	0.121	0.020	0.147	0.030	0.128	0.009	0.263	0.012	0.309	0.013	0.279	0.017	0.368	0.020	0.376	0.009
0.007	0.001	0.006	0.001	0.007	0.001	0.007	0.001	0.010	0.001	0.015	0.001	0.012	0.002	0.016	0.002	0.017	0.001
0.797	0.026	0.856	0.026	0.897	0.047	0.892	0.009	0.766	0.019	0.732	0.012	0.712	0.036	0.670	0.009	0.673	0.010
0.889	0.012	0.872	0.028	0.841	0.088	0.869	0.032	0.828	0.016	0.849	0.023	0.803	0.039	0.839	0.013	0.859	0.009
0.044	0.002	0.054	0.009	0.040	0.018	0.042	0.008	0.051	0.009	0.045	0.008	0.069	0.039	0.048	0.010	0.035	0.003
0.001	0.000	0.001	0.001	0.000	0.000	0.000	0.000	0.001	0.001	0.001	0.001	0.001	0.000	0.001	0.002	0.000	0.000
0.760	0.021	0.813	0.014	0.817	0.006	0.836	0.004	0.706	0.007	0.678	0.007	0.657	0.030	0.628	0.008	0.638	0.006

[b]Analyses of clinopyroxene which suffered subsolidus re-equilibration with high-temperature amphibole. Ions were calculated on the basis

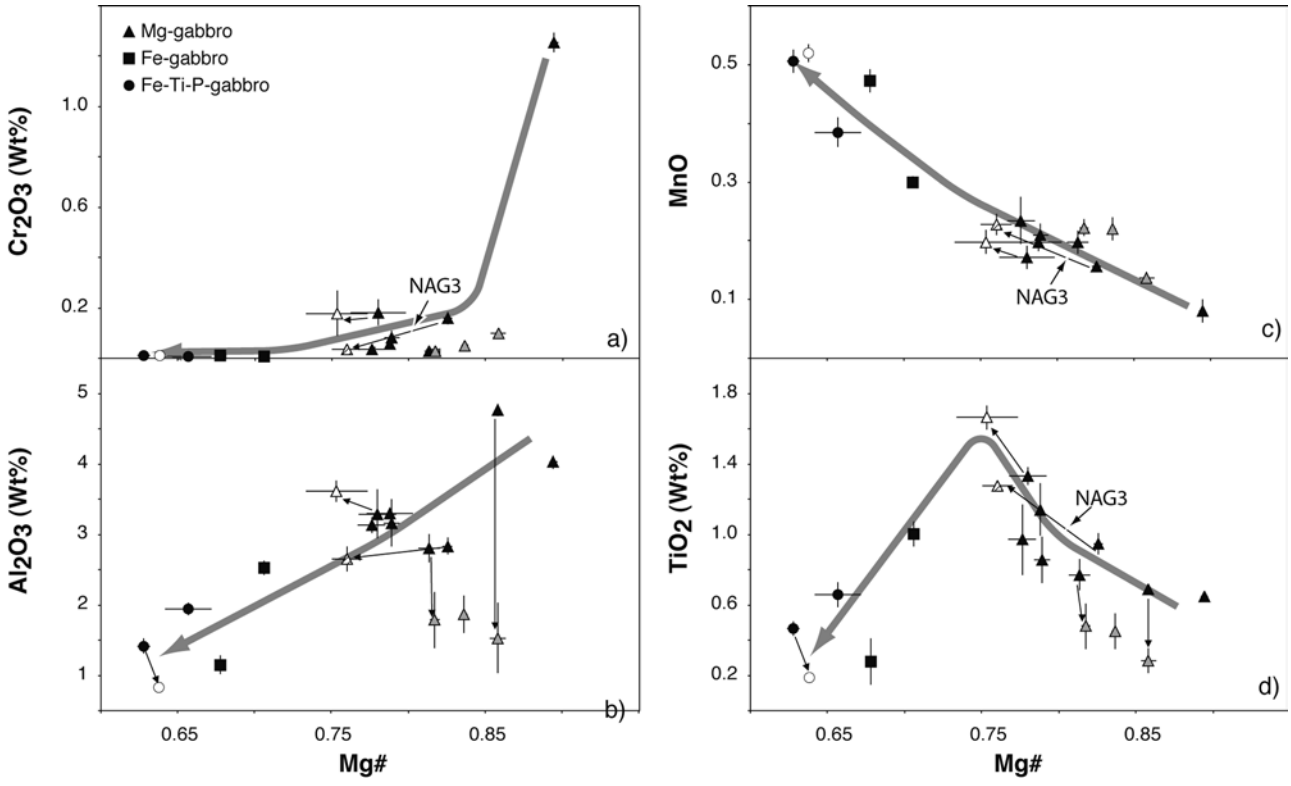

Fig. 3a–d Chemical composition of the clinopyroxene of the different gabbro types. *Shaded symbols* represent clinopyroxene which record post-cumulus re-equilibration with amphiboles, *dashed symbol* represents clinopyroxene rims and *open symbols* represent neoblastic grains. *Closed arrows* indicate the shift in composition within a single sample; *shaded arrows* indicate the differentiation trend. **a** Cr_2O_3 vs. Mg#; **b** Al_2O_3 vs. Mg#. The compatible elements continuously decrease together with Mg# from Mg- to Fe-Ti-P-gabbro. The decrease of Mg# and Cr_2O_3 from core to rim and from porphyroblast to neoblast indicates the presence of differentiated interstitial melts. Subsolidus re-equilibration of the clinopyroxene with high-temperature amphiboles leads to a decrease of Al_2O_3 but does not change the Mg# of the clinopyroxene. **c** MnO vs. Mg#. MnO continuously increases with decreasing Mg# from Mg- to Fe-Ti-P-gabbro. **d** TiO_2 vs. Mg#. TiO_2 first increases and then decreases with decreasing Mg#. This is due to the lower temperature of crystallization of the Fe- and Fe-Ti-P-gabbros. Late re-equilibration of the clinopyroxene with high-temperature amphiboles leads to a decrease in TiO_2 of the clinopyroxene (Mg# = molecular $Mg/(Mg + Fe_{tot})$)

samples. In two samples, however, clinopyroxene rims and/or neoblasts are enriched in MnO and TiO_2 and show lower Mg# and Cr_2O_3 than the composition of the core (NAG3, SC5). The general decrease of TiO_2 in cpx is probably linked to the decrease of TiO_2 in the liquid, due to Ti-oxide precipitation in Fe-Ti-gabbros whereas the core-rim variations are better explained by post-cumulus crystallization from evolved Fe-Ti-rich liquids.

Amphibole

Crystallization of interstitial Ti-pargasite is observed in all gabbro types except for the Mg-rich sample P4, but is more frequent in the differentiated gabbros (Fe-, Fe-Ti-P-gabbro and diorite; Table 2). These high-temperature amphiboles are Ti-rich calcic amphiboles characterized by high Al_2O_3 (up to 13 wt%) contents and a low Na^{M4} content (0.13–0.29 p.f.u.). They show a decrease in Mg# from Mg- to Fe-Ti-P-gabbros which correlate with a decrease in TiO_2 and CaO and with an increase in MnO. The FeO*/MgO ratio and the TiO_2 content of pargasite are positively correlated with those of clinopyroxene but are higher than those of the coexisting clinopyroxene. FeO*/MgO and Ti partitioning among amphibole and clinopyroxene indicates conditions close to equilibrium (Fig. 4a, b).

Whole-rock composition

The compositions of the different gabbro types are given in Table 3. The evolution from Mg- to Fe- and highly differentiated Fe-Ti-P-gabbro and diorite is well reflected in the change of the bulk-rock Mg# (Fig. 5). SiO_2 is roughly constant for the Mg-gabbro but decreases dramatically in the Fe- and Fe-Ti-P-gabbros and slightly increases in the diorite. The strong hydrothermal alteration and the systematic breakdown of plagioclase in all samples make it difficult to use major elements and especially the alkalies to decipher the magmatic evolution of the gabbros. Therefore, the differentiation of the gabbros will be discussed mainly on the base of their trace-element concentrations. Compatible elements such as Ni and Cr continuously decrease with decreasing Mg# whereas incompatible elements such as Ti, P, Zr, Th, and

Table 2 Chemical composition of the high-temperature amphiboles of the Platta gabbro

	Mg-gabbro										Fe-gabbro						Fe-Ti-P-gabbro								Diorite			
Sample[a]	MS8		MS13		MSG2-1				NAG5		MS3		MSG2-3		MSG2-3		P9		NAG7				MS10		MSG-2		MSG2-3	
Texture	Interstitial		Interstitial		Interstitial		Exsolution		Interstitial		Interstitial		Interstitial		Exsolution		Interstitial		Neoblastic		Interstitial		Euhedral		Euhedral		Euhedral	
SiO_2	43.75	1.73	43.22	1.38	42.58	0.29	44.03	1.75	42.87	0.72	42.59	2.35	46.44	2.01	45.45	0.97	43.14	1.24	42.96	0.36	43.03	0.08	46.20	0.44	43.03	0.08	45.60	1.91
TiO_2	3.79	0.74	3.10	0.46	3.26	0.23	2.52	0.33	2.87	0.63	3.86	0.92	2.13	0.65	2.25	0.09	2.77	0.84	2.78	0.15	2.24	0.12	2.84	0.35	2.24	0.12	2.66	0.58
Cr_2O_3	0.06	0.01	0.07	0.03	0.04	0.02	0.05	0.04	0.02	0.02	0.02	0.01	0.03	0.02	0.03	0.01	0.01	0.02	0.01	0.01	0.00	0.00	0.01	0.01	0.00	0.00	0.02	0.02
Al_2O_3	10.98	1.45	10.52	1.02	10.72	0.24	9.79	1.66	8.96	0.99	10.67	1.53	6.48	1.51	7.41	0.33	10.94	1.52	9.16	0.63	8.92	0.10	7.18	0.20	8.92	0.10	6.96	1.28
Fe_2O_3	1.60	0.73	5.78	1.59	4.20	1.15	3.83	4.92	3.88	2.45	2.44	0.67	1.89	1.13	2.02	0.53	1.40	0.67	3.74	1.07	3.87	0.51	1.01	0.38	3.87	0.51	1.51	0.86
FeO	8.72	0.33	5.62	0.95	4.93	0.45	6.73	4.50	12.67	2.28	11.63	0.93	13.05	0.27	11.31	1.30	13.45	1.33	12.91	1.17	13.79	0.23	11.66	0.20	13.79	0.23	14.45	1.34
MnO	0.12	0.01	0.12	0.02	0.15	0.02	0.19	0.03	0.34	0.04	0.19	0.10	0.49	0.01	0.38	0.02	0.21	0.04	0.31	0.02	0.32	0.03	0.42	0.04	0.32	0.03	0.52	0.08
MgO	14.90	0.42	14.76	0.51	15.92	0.19	15.11	1.75	11.57	0.56	12.69	1.15	13.31	1.26	14.02	0.64	11.68	0.48	10.94	0.42	10.59	0.09	14.58	0.19	10.59	0.09	12.20	0.93
CaO	11.51	0.42	11.35	0.23	11.49	0.17	11.61	0.76	10.02	0.31	10.98	0.42	10.46	0.41	11.12	0.51	10.79	0.33	10.53	0.12	10.92	0.05	10.94	0.19	10.92	0.05	10.10	0.65
Na_2O	2.88	0.41	2.44	0.35	3.13	0.07	2.66	0.32	2.94	0.10	2.81	0.55	2.59	0.53	2.73	0.21	3.26	0.19	2.95	0.14	2.74	0.02	2.42	0.12	2.74	0.02	2.71	0.50
K_2O	0.16	0.03	0.19	0.04	0.11	0.05	0.11	0.10	0.21	0.03	0.22	0.06	0.26	0.10	0.12	0.03	0.36	0.10	0.30	0.04	0.33	0.06	0.24	0.08	0.33	0.06	0.31	0.12
H_2O	2.08	0.00	2.06	0.03	2.05	0.01	2.05	0.03	1.98	0.02	2.03	0.02	2.02	0.03	2.02	0.03	2.05	0.02	1.98	0.03	1.98	0.00	2.04	0.01	1.98	0.00	2.00	0.02
Total	100.5	0.43	99.25	1.00	98.62	0.66	98.70	0.74	98.33	0.89	100.1	0.75	99.16	1.08	98.93	0.86	100.0	0.45	98.57	1.12	98.75	0.10	99.54	0.63	98.75	0.10	99.05	0.59
Si	6.317	0.254	6.300	0.153	6.228	0.016	6.450	0.158	6.481	0.126	6.277	0.292	6.901	0.249	6.741	0.061	6.394	0.169	6.492	0.079	6.522	0.000	6.785	0.048	6.522	0.000	6.827	0.232
Ti	0.411	0.080	0.340	0.051	0.359	0.026	0.279	0.038	0.327	0.073	0.428	0.103	0.238	0.071	0.251	0.010	0.309	0.093	0.316	0.019	0.255	0.014	0.314	0.038	0.255	0.014	0.300	0.066
Cr	0.007	0.001	0.008	0.003	0.005	0.002	0.005	0.005	0.002	0.003	0.002	0.001	0.003	0.003	0.003	0.001	0.002	0.002	0.001	0.001	0.000	0.000	0.001	0.001	0.000	0.000	0.002	0.002
Al	1.868	0.245	1.809	0.187	1.849	0.050	1.694	0.317	1.595	0.166	1.853	0.276	1.136	0.271	1.295	0.062	1.912	0.268	1.630	0.096	1.593	0.015	1.246	0.035	1.593	0.015	1.229	0.231
Fe^{3+}	0.174	0.079	0.634	0.174	0.462	0.124	0.420	0.537	0.440	0.276	0.271	0.075	0.212	0.128	0.225	0.057	0.156	0.074	0.424	0.117	0.441	0.057	0.111	0.040	0.441	0.057	0.171	0.097
Fe^{2+}	1.053	0.039	0.685	0.117	0.603	0.057	0.830	0.563	1.603	0.296	1.434	0.117	1.622	0.025	1.405	0.182	1.714	0.153	1.633	0.163	1.748	0.033	1.433	0.024	1.748	0.033	1.811	0.185
Mn	0.014	0.001	0.015	0.002	0.018	0.002	0.024	0.004	0.043	0.004	0.024	0.013	0.062	0.001	0.048	0.002	0.026	0.004	0.039	0.002	0.041	0.004	0.053	0.005	0.041	0.004	0.066	0.011
Mg	3.206	0.092	3.206	0.089	3.472	0.052	3.296	0.330	2.606	0.111	2.789	0.229	2.947	0.264	3.099	0.097	2.579	0.106	2.463	0.072	2.392	0.025	3.191	0.045	2.392	0.025	2.722	0.185
Ca	1.781	0.067	1.772	0.028	1.801	0.036	1.823	0.128	1.623	0.057	1.734	0.052	1.665	0.056	1.766	0.072	1.713	0.055	1.705	0.021	1.772	0.011	1.722	0.034	1.772	0.011	1.620	0.085
Na	0.807	0.115	0.690	0.102	0.887	0.018	0.756	0.100	0.861	0.028	0.803	0.160	0.746	0.156	0.788	0.072	0.938	0.059	0.863	0.034	0.804	0.009	0.691	0.039	0.804	0.009	0.789	0.150
K	0.029	0.004	0.036	0.007	0.020	0.010	0.021	0.020	0.040	0.007	0.042	0.012	0.048	0.020	0.023	0.007	0.068	0.019	0.058	0.008	0.063	0.012	0.044	0.014	0.063	0.012	0.058	0.023
OH	2.000	0.000	2.000	0.000	2.000	0.000	2.000	0.000	2.000	0.000	2.000	0.000	2.000	0.000	2.000	0.000	2.000	0.000	2.000	0.000	2.000	0.000	2.000	0.000	2.000	0.000	2.000	0.000
Mg#	0.724	0.012	0.709	0.017	0.765	0.021	0.724	0.046	0.560	0.015	0.621	0.034	0.616	0.039	0.656	0.026	0.580	0.026	0.545	0.014	0.522	0.006	0.673	0.008	0.522	0.006	0.579	0.037

[a]Presentation as in Table 1. Ions calculated on the basis of 23 oxygens and Σ (cat)–Ca–Na–K = 13. $Mg\# = Mg/(Fe^{3+} + Fe^{2+} + Mg)$

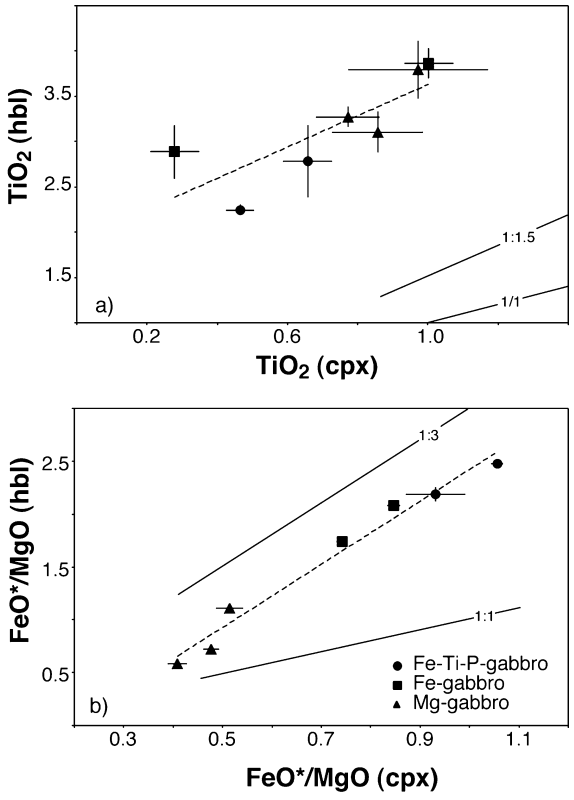

Fig. 4 **a** TiO_2 and **b** FeO*/MgO partitioning between clinopyroxene and amphibole. Contours of K_d^{Ti} (amp–cpx) indicate equilibration between clinopyroxene and amphibole

U increase. Two samples (NAG9, a Mg-gabbro and MS3, a Fe-gabbro) fall off the general trend. NAG9 is strongly enriched in U and Th and MS3 is enriched in Ti. These features suggest open-system post-cumulus crystallization of differentiated liquids within both samples.

The highly differentiated Fe-Ti-P-gabbros and the diorite display low Mg# and show complementary trace-element compositions. The Fe-Ti-P-gabbros show higher concentrations in Ti, P, V, and Mn which are mainly incorporated in ilmenite and apatite. SiO_2, Al_2O_3, Zr, U, and Th are preferentially concentrated within the diorite and are incorporated in plagioclase and zircon, respectively.

Gabbros from Fuorcla da Faller and Val da Natons display contrasting REE patterns (Fig. 6). The gabbros from Fuorcla da Faller show parallel REE patterns with an increase of REE concentrations with decreasing Mg#. The Mg- and Fe-gabbros display positive Eu, Ba and Sr anomalies which decrease with Mg# and become negative for the highly differentiated diorite and Fe-Ti-P-gabbros (Fig. 6a, c). The Fe-gabbro (MS3) is also characterized by a positive anomaly in Ta, Nb and Ti (Fig. 6c).

The gabbros from Val da Natons display more variable REE patterns (Fig. 6b). The primitive Mg-gabbros (P6) display rather flat patterns similar to N-MORBs with no Eu and Ba positive anomalies. This indicates the absence of cumulate plagioclase in this sample. Sr is slightly negative and may reflect late alteration processes during breakdown of plagioclase. The clinopyroxene and plagioclase of sample P6 show graphic intergrowth indicating cotectic crystallization of the two phases, and supporting the interpretation that P6 represents a gabbroic frozen melt. By contrast, although sample NAG3 does not show any Eu and Sr positive anomalies, it is composed of cumulus phases and trapped liquid, as indicated by the core-rim chemical variations of its clinopyroxene (Fig. 3) and by the crystallization of ilmenite. The crystallization of this phase may be responsible for the enrichment in LREEs and incompatible elements of this sample during late infiltration of oxide-gabbro into a cumulus Mg-gabbro. Another Mg-gabbro (NAG9) shows a fairly high REE concentration compared to its Mg#. It is particularly enriched in HREEs and most incompatible elements and shows a small positive Eu anomaly. The enrichment in HREEs, U, Th, Ta, Nb and Hf suggests a possible late reaction with and/or infiltration by dioritic liquids. However, sample NAG9 contains primitive clinopyroxene cores with Mg# of 0.86. Only the Fe- and Fe-Ti-P-gabbro and the diorite show REE concentrations and patterns similar to the Fuorcla da Faller samples. At both localities, the diorite and the Fe-Ti-P-gabbro show complementary REE concentrations. Diorites are enriched in HREEs and depleted in MREEs and LREEs relative to the Fe-Ti-gabbros.

Basalts and dolerite

Field relationships

Basaltic rocks cover a large area in the Platta nappe (Fig. 1b). They occur as massive basaltic flows, pillow lavas, pillow breccias, hyaloclastites and individual dolerite dykes cutting across serpentinized peridotites and locally gabbroic rocks, showing chilled margins against the country rocks (Dietrich 1969; Desmurs et al. 2001). Most of the basalts occur in the lower serpentinite unit, being limited to one basaltic flow and a few dolerite dykes within the upper serpentinite unit. They seem to be the youngest magmatic rocks emplaced in the Platta nappe, as they overly serpentinites and gabbro breccias. However, the relative timing of emplacement of basalt and gabbros can not be unambiguously deciphered from field relationships alone (Desmurs et al. 2001).

Petrography

The massive basaltic flows and the dolerites show an intersertal to intergranular texture with interstitial clinopyroxene and round patches of chlorite which may represent former olivine. Low-grade alteration is widespread in all samples; olivine and plagioclase are completely altered. In a few samples, interstitial brown hornblende and oxide occur as well as few acicular grains of apatite. The pillow basalts can be coarsely

Table 3 Major- and trace-element composition of the Platta gabbros

Sample[a]	Mg-gabbro							Fe-gabbro		Fe-Ti-P-gabbro		Diorite	
	P6	NAG3	NAG9	P4	MS15	MS9	MS13	NAG5	MS3	NAG7	P9	MS10	P7
SiO_2	49.55	51.87	52.75	46.95	48.59	49.79	49.92	43.30	44.13	39.76	34.50	52.23	55.12
Al_2O_3	13.97	17.04	13.96	23.19	16.75	16.28	15.77	12.81	10.55	12.38	9.98	17.56	18.82
Fe_2O_3	7.68	6.93	4.18	2.61	5.70	6.21	5.48	15.47	11.47	17.18	22.44	6.33	4.77
MnO	0.13	0.14	0.07	0.05	0.10	0.10	0.10	0.19	0.20	0.29	0.32	0.07	0.07
MgO	9.51	5.17	9.55	7.42	8.34	8.43	7.96	5.97	13.58	6.54	8.29	3.03	3.28
CaO	11.78	7.96	10.17	8.59	12.28	10.91	13.36	10.10	9.26	11.95	10.20	11.71	9.72
Na_2O	3.43	5.51	4.74	2.91	3.24	3.81	3.40	3.26	2.25	2.44	1.97	5.57	5.99
K_2O	0.15	0.91	0.29	2.60	0.69	0.46	0.29	0.13	0.00	0.00	0.00	0.00	0.11
TiO_2	0.71	1.49	0.23	0.11	0.47	0.60	0.37	6.40	3.88	3.86	5.27	1.01	0.38
P_2O_5	0.16	0.32	0.09	0.08	0.09	0.09	0.08	0.14	0.12	1.90	2.58	0.28	0.10
LOI	2.75	2.51	3.82	5.38	3.61	3.14	3.08	2.22	4.39	3.20	3.45	2.09	1.50
Total	99.82	99.85	99.85	99.89	99.86	99.82	99.81	99.99	99.83	99.51	99.04	99.90	99.86
Mg#	0.71	0.60	0.82	0.85	0.74	0.73	0.74	0.43	0.70	0.43	0.42	0.49	0.58
Trace elements (ppm)													
V	265	202	87.6	38.5	198	179	169	869	532	290	398	77.5	117
Cr	163	1456	365	1031	50.83	84.5	135	44.8	79.7	24.4	7.21	0.00	132
Ni	138	40.5	216	352	81.7	101	83.5	76.6	87.6	23.62	39.2	15.3	42.0
Co	54.5	24	29.8	25.1	35.0	33.7	33.3	53.1	39.6	16.98	48.2	13.2	17.9
Cu	106	81.4	47.6	21.7	47.7	27.2	46.0	70.6	38.5	30.25	31.1	22	8.30
Zn	71.6	58.8	20.7	15.4	30.1	38.5	25.5	111	76.6	156	125	32.2	34.1
Zr	73.3	145	26.6	3.66	32.5	86.9	11.7	72.6	59.9	91.06	70.1	621	238
Y	32.3	28.7	13.9	2.33	14.1	18.6	9.27	17.6	19.3	115	124	120	81.2
Hf	1.89	2.98	1.64	0.12	0.85	1.92	0.44	1.79	1.50	2.44	1.74	14.2	7.39
Th	0.05	0.636	0.604	0.015	0.078	0.033	0.102	0.027	0.018	0.112	0.089	1.010	1.570
U	0.022	0.227	0.264	0.005	0.034	0.016	0.016	0.035	0.012	0.071	0.058	0.457	0.893
Ba	3.33	249	25.5	191	38.8	7.01	15.8	41.8	5.11	9.88	3.56	8.29	3.38
Rb	2.27	23.17	5.13	45.21	11.04	4.51	5.34	5.39	bdl	bdl	bdl	bdl	1.56
Sr	92.8	272	526	82.0	844	326	363	1,271	218	794	116	829	780
Nb	1.11	8.05	7.45	bdl	0.74	0.75	0.14	2.55	1.86	4.31	4.40	10.1	14.47
Ta	0.08	0.60	0.86	bdl	0.05	0.05	0.01	0.23	0.17	0.40	0.41	0.95	1.55
REEs (ppm)													
La	3.17	8.56	1.72	0.36	1.01	1.45	0.58	0.94	1.04	19.23	18.65	17.95	22.95
Ce	10.81	22.06	5.31	1.05	3.33	5.01	1.91	3.40	3.71	66.84	68.00	55.73	58.86
Pr	1.88	3.21	0.71	0.18	0.62	0.90	0.37	0.68	0.82	11.31	12.42	9.33	6.92
Nd	9.93	14.71	3.46	0.80	3.71	5.37	2.22	4.07	4.64	65.26	72.04	47.59	28.76
Sm	3.50	4.07	1.02	0.26	1.31	1.79	1.02	1.91	2.11	20.72	21.96	14.86	7.26
Eu	1.44	1.46	0.45	0.39	0.83	0.94	0.64	0.83	1.10	5.65	5.88	4.81	1.95
Gd	4.92	4.70	1.39	0.31	2.02	2.52	1.42	2.68	2.86	24.43	26.67	17.94	7.55
Tb	0.80	0.80	0.30	0.06	0.33	0.39	0.24	0.42	0.47	3.57	3.77	2.96	1.41
Dy	5.07	4.73	1.97	0.41	1.99	2.53	1.52	2.74	3.07	19.64	21.26	19.25	9.77
Ho	1.06	0.99	0.43	0.08	0.46	0.59	0.35	0.58	0.64	4.15	4.18	4.61	2.31
Er	2.82	2.84	1.37	0.23	1.41	1.70	0.91	1.61	1.73	10.47	10.44	13.04	7.08
Tm	0.44	0.43	0.27	0.04	0.18	0.24	0.13	0.25	0.25	1.39	1.32	1.85	1.32
Yb	2.76	3.01	2.18	0.22	1.32	1.79	0.83	1.66	1.79	7.92	7.71	13.25	9.95
Lu	0.45	0.41	0.37	0.03	0.21	0.27	0.13	0.24	0.26	1.17	1.14	1.98	1.53

[a]Major elements measured by emission ICP, trace elements and REEs by ICP-MS, and U and Th by ICP-MS after chromatographic separation. Bdl, below detection limit. LOI, loss on ignition

plagioclase phyric or aphyric. The aphyric pillow lavas are variolitic and exhibit the classical variation from intersertal to divergent and arborescent texture from core to rim (Dietrich 1969). The phyric pillow basalts contain albite phenocrysts (pseudomorphs after primary plagioclase) within a recrystallized ground mass of fine-grained albite, chlorite, pumpellyite, epidote, actinolite and calcite (Dietrich 1969).

Whole-rock chemistry

The whole-rock major- and trace-element composition of basaltic rocks are given in Table 4. Additional analyses may be found in Frisch et al. (1994). The major-element abundances indicate an olivine-tholeiite composition, similar to ophiolite basalts from other occurrences in the Alps and northern Apennines (Venturelli et al. 1981; Vannucci et al. 1993; Puschnig 2000; Bill et al. 2000). The basalts from the Platta ocean-continent transition show positive correlations of Mg# with Ni and Cr, and negative correlations with P_2O_5 and TiO_2 (Fig. 7). The large range of MgO (4.52–10.32 wt%) indicates that most basalts record differentiation processes and only a few samples provide evidence of being primitive liquids. The Platta basalts are characterized by two groups of different REE chondrite-normalized patterns, one with Ce_n/Sm_n and $Ce_n/Yb_n > 1$, and a second

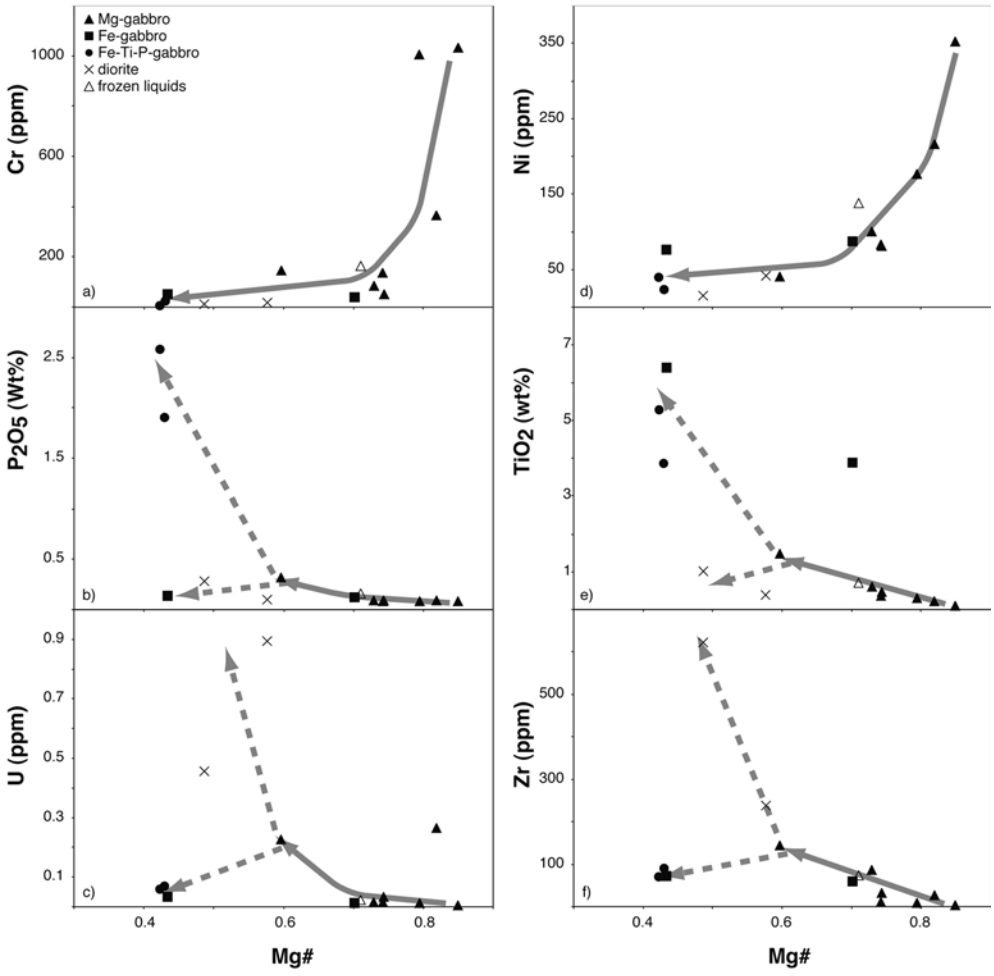

Fig. 5a–f Variation diagrams for bulk major and trace elements in the Platta gabbros. *Arrows* indicate the differentiation trend. **a** Cr vs. Mg#; **b** P_2O_5 vs. Mg#; **c** U vs. Mg#; **d** Ni vs. Mg#; **e** TiO_2 vs. Mg#; and **f** Zr vs. Mg#. The compatible elements such as Ni and Cr continuously decrease with decreasing Mg# whereas the incompatible elements increase during differentiation. Note the 'split' of the differentiation trend for P_2O_5, TiO_2, U and Zr between the Fe-T-P-gabbro and the diorite (see text for discussion). The *closed symbols* represent 'cumulates', the *open symbols* represent liquid compositions (see text)

one with Ce_n/Sm_n and $Ce_n/Yb_n < 1$. Similarly, the Nb_n/Zr_n and Th/Hf ratios are higher in the first group (0.89–1.39 and 0.17–0.26, respectively) than in the second one (0.24–0.28 and 0.03–0.05, respectively). These features are common to other basalts from the ocean-continent transition and suggest T- to N-MORB affinity (Frisch et al. 1994; Puschnig 2000).

Discussion

Primitive liquids in ocean-continent transitions

Most MORBs which erupted on the seafloor have been modified from their primary composition by fractional crystallization during ascent (e.g., Grove et al. 1992). This greatly complicates the determination of primary liquids which were in equilibrium with the mantle source. In order to test whether any of the analyzed basalts and/or gabbroic rocks from the ocean-continent transition could represent near-primary liquids, we calculated olivine compositions for primitive basalts with MgO > 8 wt% by using the K_d Fe-Mg-olivine liquid which is near 0.3 at low pressure for a wide variety of liquid compositions (Roeder and Emslie 1970; Ulmer 1989). All data are normalized on an anhydrous basis and $Fe^{3+}/\Sigma Fe = 0.05$ (Christie et al. 1986) was used. Because of the altered nature of the basalts, we applied a second criterion to check for a possible primary nature of the basalt. Ni is highly compatible in olivine and is therefore a sensitive criterion to account for olivine fractionation. We used the Ni content of the basalts and the equation of Kinzler et al. (1990) to calculate the Ni content of the equilibrium olivine. As can be seen from Fig. 8, there are just a few compositions which satisfy a 'mantle criterion' (Ni: 2,500–3,500 ppm, Mg# of olivine: 0.88 to 0.91) of being liquids in equilibrium with mantle olivine. Gabbro sample P6 is close to a primary liquid. Correction for crystal fractionation shows that about 4% of equilibrium olivine has to be added to P6 in order to obtain a composition which falls within the field of mantle olivine (Fig. 8). These primitive liquids have been considered further in the discussion about the origin of the mafic rocks in the Platta nappe.

The trace-element compositions of the primitive liquids consisting of a basalt from the upper serpentinite unit (FAB1), one gabbroic frozen melt from the lower serpentinite unit (P6), and one basalt from the adjacent Forno unit (C14, Puschnig 2000) are represented in a chondrite-normalized trace-element diagram (Fig. 9a).

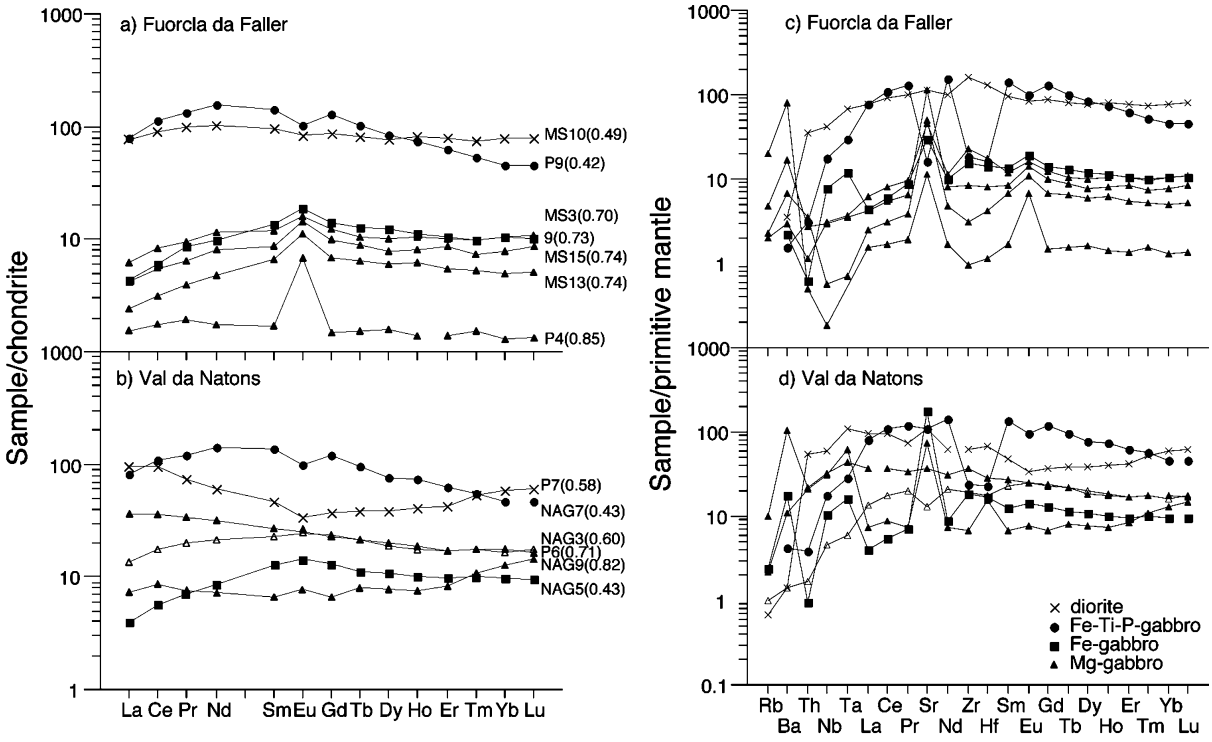

Fig. 6a–d REE and trace element patterns of different gabbro types from Fuorcla da Faller and Val da Natons in the Platta nappe. **a, b** Normalization to C1 chondrite, and **c, d** normalization to primitive mantle (Sun and McDonough 1989). The *closed symbols* represent cumulates, the *open symbols* represent frozen melts (see text). *Values in parentheses* indicate Mg# (Mg# = Mg/(Mg + Fe_{tot}))

These liquids show distinct patterns. The primitive basalt from the upper serpentinite (FAB1) is enriched in LREEs, and other incompatible elements (Ta, Nb) compared to the MREEs and HREEs, and it is characterized by a $(La/Sm)_N > 1$ similar to T-MORB as well as by a positive Zr anomaly. The primitive gabbroic frozen liquid (P6) from the lower serpentinite unit is depleted in incompatible elements relative to LREEs, shows no Zr anomaly and HREE typical of N-MORB. The large differences in REEs and other incompatible elements among the primitive liquids (Mg# 0.7 to 0.73, Ni: 2,500 to 3,500 ppm) can not be explained by fractional crystallization nor by possible effects of trapped liquids but rather reflect heterogeneity in the mantle source (see below). Indeed, simple modeling of low-pressure fractional crystallization (see below) led to an overall enrichment of the incompatible elements, but not to a strong fractionation between the HREEs and the LREEs, considering liquids with $(La/Sm)_N > 1$ (Fig. 9b) and $(La/Sm)_N < 1$ (Fig. 9c), respectively. Another interesting observation regarding Fig. 9 is that most samples show a positive Zr anomaly with respect to the neighboring REEs. Such a trace-element pattern is not uncommon in basalts and is a characteristic feature of low-degree melts generated in the spinel peridotite field (e.g., Casey 1997).

Gabbroic rocks: frozen liquids versus crystal fractionation

Field relations and whole-rock chemistry of the gabbros show unambiguously that each individual gabbro occurrence represents a single batch of melt emplaced within the serpentinites.

The gabbros of the Fuorcla da Faller area show a continuous evolution from olivine-bearing Mg-gabbro to highly differentiated diorite and Fe-Ti-P-gabbros. This evolution is well imaged by the increase in accessory minerals and the continuous decrease of the Mg#, which correlate with the increase of the bulk REEs without marked changes in the modal abundance of plagioclase and clinopyroxene. Fractional or in-situ crystallization (cf. Langmuir 1989) is most probably the dominant process (see also modeling of crystal fractionation below). The strong enrichment of bulk Ti and Fe of sample MS3 is most probably derived from iron- and titanium-rich late magmatic liquids expelled by compaction from deeper-seated olivine-gabbro cumulates (open-system crystallization).

Gabbros in Val da Natons show a crystallization history different from that of Fuorcla da Faller in that their REE content does not correlate with the Mg# of the whole rock. Sample P6 has REE patterns close to a crystallized liquid. Sample NAG9 displays a low degree of differentiation but is enriched in HREEs, U, Th and Zr. The liquids producing such a signature are most likely those of zircon-rich diorites which occur as small veins within this particular outcrop. Despite the evidence of the infiltration of dioritic liquids, this sample

Table 4 Major- and trace-element composition of the Platta basalts

Sample	Lower unit								Upper unit	
	P8	P5	C14[a]	OE73[b]	OE74[b]	201[b]	SGO4[b]	SGO5[b]	PCD1	FAB1
SiO_2	47.19	48.17	47.77	50.54	46.83	48.32	47.61	48.01	49.49	47.35
TiO_2	1.69	1.82	0.96	1.92	2.29	2.18	1.33	1.26	1.72	1.46
Al_2O_3	14.99	15.88	16.98	16.46	14.53	15.58	19.78	16.61	17.01	15.67
Fe_2O_3	9.11	9.91	7.94	8.48	12.04	10.12	10.37	7.83	8	8.83
MnO	0.15	0.16	0.12	0.11	0.21	0.12	0.17	0.13	0.11	0.13
MgO	5.54	6.58	9.33	4.33	5.20	7.36	8.56	7.47	6.23	9.76
CaO	10.5	9.78	11.41	8.12	9.05	5.92	2.82	10.12	8.58	8.11
Na_2O	4.36	4.3	2.22	5.47	3.09	4.01	5.42	3.50	5.02	2.86
K_2O	0.76	bdl	0.06	0.47	bdl	1.32	0.55	0.87	0.06	0.12
P_2O_5	0.27	0.25	0.10	0.34	0.36	0.31	0.15	0.12	0.32	0.28
LOI	5.27	2.98	1.56	3.50	6.35	3.32	4.61	3.42	3.28	5.27
Total	99.83	99.83	98.54	99.75	99.95	98.56	101.37	99.34	99.82	99.84
Mg#	0.55	0.57	0.70	0.50	0.46	0.59	0.62	0.65	0.61	0.69
Trace elements (ppm)										
V	245	259	166	204	283	260	131	187	202	170
Cr	242	188	430	114	118	141	265	249	151	277
Ni	82	95	191	91	58	67	213	110	81	209
Co	34	31	30	–	–	–	–	–	30	45
Cu	60	39	42	–	–	–	–	–	50	52
Zn	84	78	51	–	–	–	–	–	73	74
Zr	169	158	53	227	216	271	85	106	184	132
Y	38	36	10	33	43	40	24	–	29	23
Hf	4.14	3.78	–	–	–	–	–	–	4.11	2.72
Th	0.19	0.18	–	–	–	–	–	–	0.72	0.70
U	0.12	0.07	–	–	–	–	–	–	0.27	0.23
Ba	28	7.54	–	107	81	83	50	68	44	38
Rb	18	bdl	–	15	16	17	bdl	4.10		
Sr	82	94	142	301	177	285	78	230	212	175
Nb	2.66	2.80	–	–	–	–	–	–	10.94	11.53
Ta	0.23	0.24	–	–	–	–	–	–	0.77	0.75
REEs (ppm)										
La	5.84	5.73	2.74	11	10	8	2	3	10.18	8.95
Ce	19.25	18.52	7.31	27	26	22	5	10	25.14	21.47
Pr	3.20	3.03	1.35	–	–	–	–	–	3.49	2.77
Nd	15.74	14.46	7.43	19	24	21	–	–	15.67	12.38
Sm	4.86	4.39	2.77	5.3	7.2	6.2	2.2	2.9	4.29	3.35
Eu	1.70	1.66	1.18	1.6	2.1	1.8	0.9	1.1	1.44	1.26
Gd	5.89	5.16	3.71	–	–	–	–	–	4.52	3.77
Tb	0.94	0.84	0.50	–	–	–	–	–	0.76	0.62
Dy	6.11	5.64	3.66	–	–	–	–	–	4.85	3.62
Ho	1.37	1.27	0.79	–	–	–	–	–	1.04	0.76
Er	3.52	3.28	2.21	–	–	–	–	–	2.77	2.05
Tm	0.54	0.52	0.32	–	–	–	–	–	0.45	0.33
Yb	3.57	3.29	2.04	4	5	5	3	2	2.94	2.00
Lu	0.60	0.53	0.28	0.5	0.7	0.6	0.4	0.3	0.49	0.28

[a]Sample from the Forno unit (Puschnig 2000)
[b]Samples from Frisch et al. (1994). –, Not analyzed, bdl, below detection limit. LOI, loss on ignition

has clinopyroxene with Mg# of 0.86, a LREE-depleted pattern and no Eu anomaly (Desmurs and Müntener, unpublished data), indicating that the cumulus clinopyroxene crystallized from fairly primitive liquids. Late-stage infiltration of oxide-rich gabbros could explain chemical variations of clinopyroxene crystals in sample NAG3. Pronounced core-rim zoning of Mg#, Cr_2O_3 and TiO_2 in clinopyroxene indicates that the rim crystallized from evolved liquids, most likely from oxide-rich liquids. This is supported by the high modal amounts of ilmenite and an incompatible element-rich whole-rock composition (Table 3).

Parental melts of the gabbros

The parental melts of the gabbros can be calculated by dividing the most primitive clinopyroxene compositions by crystal-liquid distribution coefficients. This procedure assumes that the clinopyroxenes retained the composition of crystals in equilibrium with a liquid. Calculated liquid compositions from the most primitive samples (P4, NAG9) are strikingly similar to the measured composition of some gabbros which represent a frozen liquid (P6) and are relatively primitive N-MORB (sample P6, Mg# = 0.70). Parental melts of Jurassic gabbros

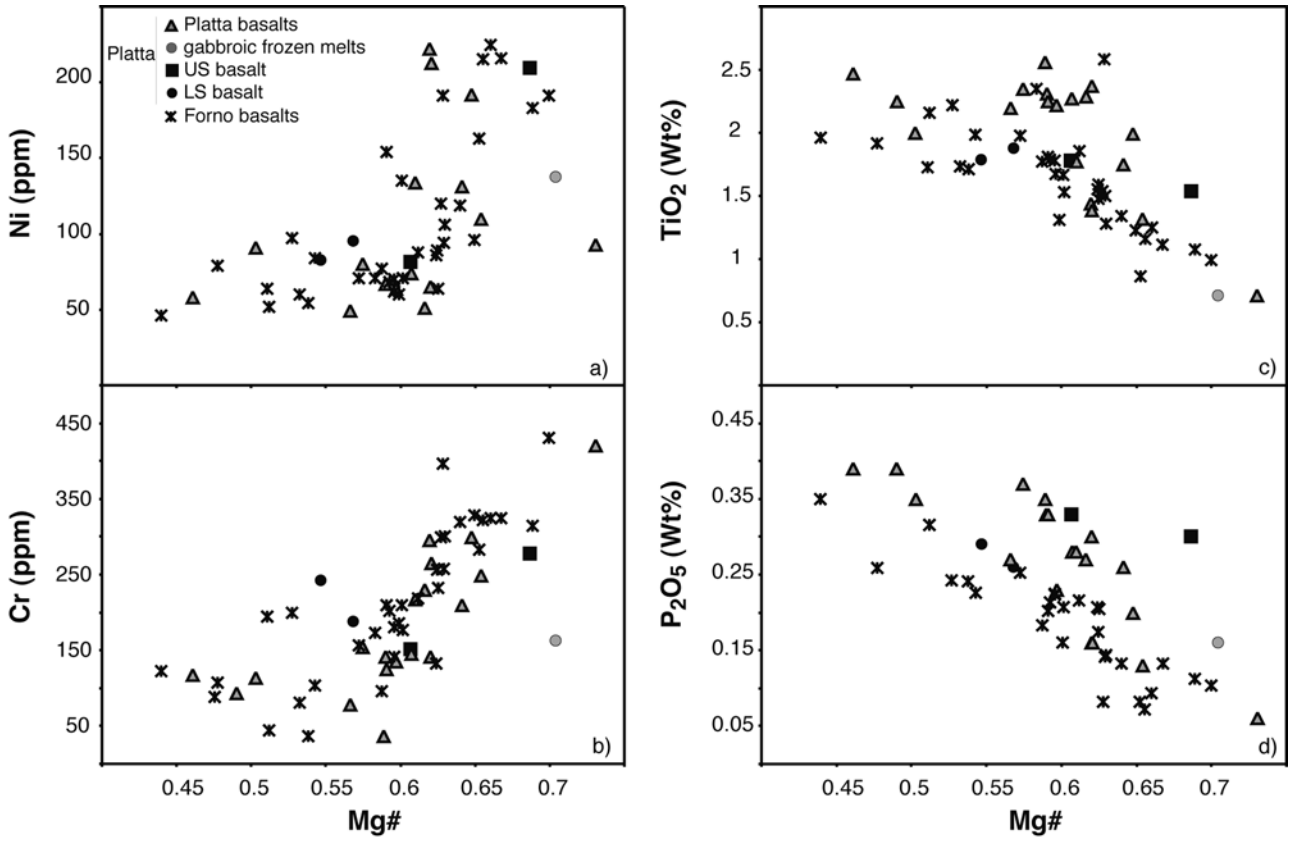

Fig. 7a–d Variation of compatible and incompatible elements of the Platta basalts with Mg#. **a** Ni vs. Mg#; **b** Cr vs. Mg#; **c** TiO_2 vs. Mg#; and **d** P_2O_5 vs. Mg#. The compatible elements Cr and Ni continuously decrease and the incompatible elements Ti and P increase with decreasing Mg#. The Forno basalts are from Puschnig (2000), the Platta basalts from Frisch et al. (1994). *US* Upper serpentinite unit, *LS* lower serpentinite unit of the Platta nappe

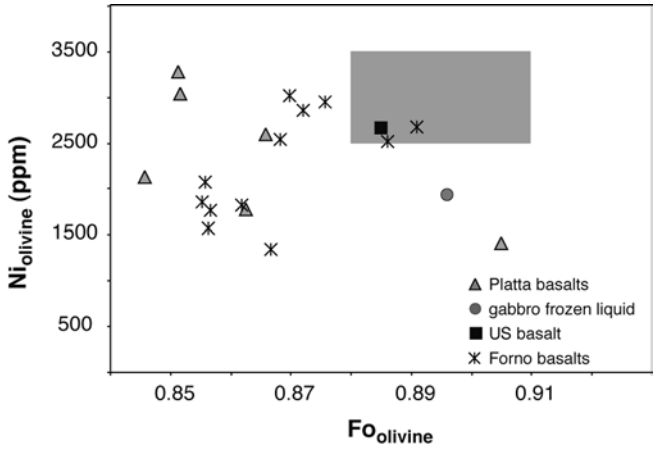

Fig. 8 Ni and forsterite content of the calculated olivine in equilibrium with Platta and Forno basalts with MgO > 8 wt%. The forsterite content was calculated using a K_d FeO*/MgO of 0.3 (Roeder and Emslie 1970; Ulmer 1989), and the Ni content was calculated using the equations of Kinzler et al. (1990) and $Fe^{3+}/Fe_{tot} = 0.05$ (Christie et al. 1986). *Shaded field* Composition of olivine from abyssal peridotites (see text for discussion)

from the internal Ligurides calculated from the composition of clinopyroxene from olivine-gabbros show N-MORB affinities, too (Tiepolo et al. 1997; Tribuzio et al. 1999).

Modeling crystal fractionation

Simple modeling of closed-system fractional crystallization of a liquid with a P6 composition using the MIXNFRAC software written by Roger Nielsen (http://EarthRef.org/GERM/bottom.htm) successfully matches the mineralogy and trace-element composition of the Fuorcla da Faller 'cumulates'. As an initial liquid for modeling, we have chosen sample P6 which is close to a near-primary liquid (Fig. 9a). Modeling shows that olivine-gabbros formed after 10% crystallization of olivine cumulates and troctolites. Between 15 and 70% crystallization, clinopyroxene-plagioclase gabbros with less than 5% olivine are formed. Above ca. 75% crystallization, the model predicts the occurrence of a Fe-Ti-oxide within the cumulate pile, and apatite appears after about 85% crystallization. This crystallization sequence is consistent with the one found in the field. Furthermore, the model predicts no crystallization of orthopyroxene, which is also consistent with observations in the Fuorcla da Faller gabbro. The trace-element patterns of the cumulate predicted by the model agree reasonably well with the ones observed (Fig. 10). It shows that the most primitive olivine-gabbro formed after about 12%

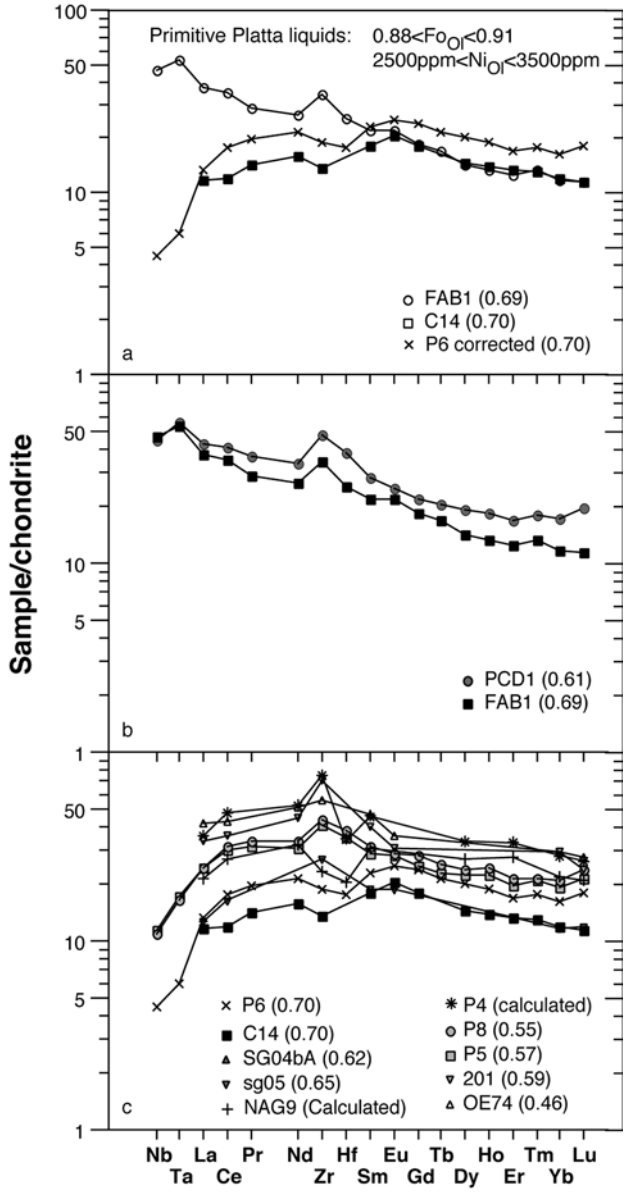

Fig. 9 **a** Trace-element compositions of the most primitive basaltic liquids of the Platta nappe. **b** Trace-element composition of T-MORB, and **c** N-MORB of the Platta nappe. *Crosses* represent gabbroic parental melts. Samples NAG 9 and P4 are calculated from their clinopyroxene composition (Desmurs and Müntener, unpublished data) using the partition coefficient of Hart and Dunn (1993). Composition of sample C14 is from Puschnig (2000), of samples SG04a, SG05, OE74 and 201 from Frisch et al. (1994). Normalization is to C1 chondrite (Sun and McDonough 1989)

of fractional crystallization. The REE pattern of the Mg-gabbros of the Fuorcla da Faller match the one predicted by the model between 20 and 70% of fractional crystallization. The predicted composition of the cumulate after 90% crystallization closely mimics the one of the Fe-Ti-P-gabbro, and the composition of the residual liquid matches the one of the diorite (Fig. 10). If the mineralogy and the trace elements of the gabbros are well simulated by the model, this is not the case for the major elements, especially for the most differentiated rock types. Indeed, the model predicts much more fractionated compositions in terms of Mg# numbers than the ones observed in the most differentiated rocks. This is due to the presence of small quantities of interstitial liquids within some gabbro cumulates which equilibrated with the cumulus phases and which are not simulated by the model. This is illustrated by the Fe-gabbro MS3 which is particularly enriched in Ti and trace elements with respect to its whole-rock Mg# of 0.70 (Fig. 5). Such a signature suggests infiltration of late Ti-rich liquids into previously crystallized cumulate gabbros, leading to crystallization of ilmenite and to an increase in incompatible elements such as Nb and Ta. Thus, the genesis of Fuorcla da Faller gabbros could be explained by a process of fractional crystallization coupled with late percolation of differentiated liquids expelled from deeper-seated olivine-gabbro cumulates.

A similar process has been proposed to explain the chemical variability of gabbros from hole 735b drilled during ODP leg 176 (Dick et al. 2000). The mineralogy and stratigraphy of the gabbros drilled at this location of the SW Indian Ridge is similar to that of the Fuorcla da Faller gabbro, although the volume of the gabbros cannot be compared. Magma production rates must be much higher along slow-spreading ridges compared to passive margin settings. This indicates that the Fuorcla da Faller gabbros represent the earliest stages of a slow-spreading system whereas 735b represents an example of a mature slow-spreading ridge.

Variation of degree and sources of melting

The volume of the mafic rocks is much larger in the lower and originally oceanward serpentinite unit than in the upper unit (Fig. 1). Furthermore, their chemistry is different, with T-MORB affinities dominating in the upper serpentinite unit and N-MORB chemistry in the lower one. The two groups of basalts show different ratios of incompatible elements such as Nb/Zr and Th/Hf, suggesting that they originated from different sources. In Fig. 11a, the Nb_n/Zr_n and Ce_n/Sm_n ratios of the Platta basalts are plotted and compared to basalts from other Liguria-Piedmont ophiolites and the Iberia passive margin. The Platta T-MORBs are characterized by high ratios of Nb_n/Zr_n and Ce_n/Sm_n similar to the basalts from the Gets nappe which are associated with continental fragments and are characterized by low $\epsilon Nd_{(166)}$ (4.5–5.9; Bill et al. 2000). The Platta N-MORBs have ratios similar to the basalts from the Ligurides and Corsica and are characterized by variable ratios of Ce_n/Sm_n and generally low Nb_n/Zr_n, respectively. Both Platta N-MORBs and basalts from the Ligurides have high $\epsilon Nd_{(160)}$ (+7.8–9.8) indicating an asthenospheric mantle source (Stille et al. 1989; Rampone et al. 1998; Schaltegger et al. 2002). The basalts from Liguria-Piedmont ophiolites show a positive anomaly in Zr (Fig. 11b) which indicates a low degree of melting in the spinel field (Casey 1997). The Zr anomaly is positive for the Platta basalts

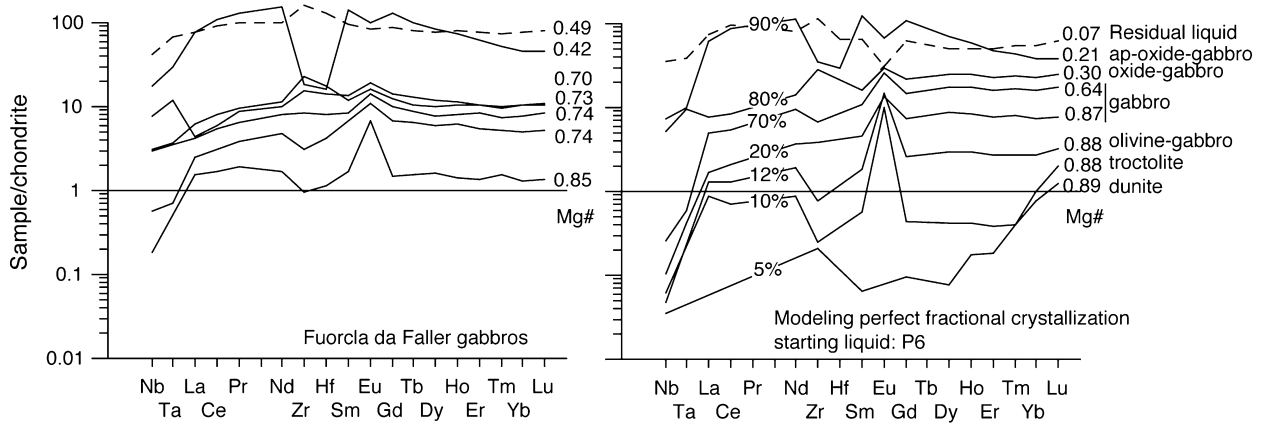

Fig. 10 Comparison of the trace-element patterns and Mg# of the Fuorcla da Faller gabbro (*left*) with the results of modeled fractional crystallization of a melt with a P6 composition (*right*; MIXNFRAC software, Nielsen). *Values* indicate the percentage of solid phases. *Dashed lines* represent the composition of the diorite of the Fuorcla da Faller gabbro (*left*), and of the calculated composition of residual liquid after 90% crystallization (*right*). Normalization is to C1 chondrite (Sun and McDonough 1989)

(1.1–1.5) and does not change from T- to N-MORB, indicating that both groups represent relatively low degrees of melting. By contrast, the Zr* decreases from T- to N-MORBs in Corsica and in the Ligurides, indicating that they are the products of variable degrees of partial melting (higher for the N-MORBs than the T-MORBs). These data support the idea that the basalts from the Liguria-Piedmont ophiolites record two processes: first, a shift from a slightly enriched (lithospheric) mantle to a depleted (asthenospheric) mantle source, and second, an increasing degree of melting in the latter source, which seems to correlate with the paleotectonic position of basalt flows in the corresponding unit.

Similarly, magmatic rocks from the present-day ocean-continent transition of the Iberia passive margin show contrasting chemistry. Based on Nd and Hf isotopes, it has been shown that syn-rift intrusive rocks crystallized from liquids with an enriched-to-depleted mantle source within the same segment of the margin (Schärer et al. 1995; Charpentier et al. 1998; Schärer et al. 2000). Basalts and dolerite from the Galicia bank (Kornprobst et al. 1988; Charpentier et al. 1998) and the Iberia abyssal plain have E-MORB signatures (Seifert et al. 1997; Cornen et al. 1999) and are characterized by high Ce_n/Sm_n and Nb_n/Zr_n ratios (Fig. 11) indicating an enriched mantle source. Basalts and dolerites from the Gorringe bank (Cornen et al. 1999) show Ce_n/Sm_n and Nb_n/Zr_n ratios similar to those of basalts from the Liguria-Piedmont ophiolites (Fig. 11). Dolerite dikes of Mt Ormonde have incompatible-element ratios similar to those of the Gets nappe and of the upper serpentinite unit in the Platta nappe, whereas dolerites from the more oceanward Mt Gettysburg have ratios similar to N-MORBs. Gabbros from this location also have a similar depleted mantle source, indicating a shift from a slightly enriched to a depleted mantle source as the magmatic rocks crystallized in a more oceanward position.

Implications for magmatism in ocean-continent transitions

The occurrence of small and isolated gabbro bodies as well as the regional variability of volumes of basaltic rocks indicate that magmatism within the Platta ocean-continent transition is quite different from that at a slow-spreading ridge as, for example, the southwest Indian Ridge (ODP site 735b; Dick et al. 2000) or the MARK area (Karson and Lawrence 1997). Indeed, even the most amagmatic segments of slow-spreading ridges such as the MARK area (Karson and Lawrence 1997) contain kilometer-sized gabbroic intrusions which can not be compared with the small volume of plutonic mafic rocks occurring along an ocean-continent transition. Similarly, magmatic rocks of slow-spreading ridges are the result of higher degrees of melting than the ones occurring along ocean-continent transitions. Such isolated, small-scale occurrences of igneous rocks could be an explanation for the weak magnetic anomalies found within the ocean-continent transition of the Iberian margin (Whitmarsh et al. 2001).

Jurassic Alpine ophiolites have often been compared with slow-spreading ridges (e.g., Lagabrielle and Lemoine 1997) but the occurrence of isolated magmatic rocks and the subcontinental origin of the ultramafic basement rather point to an ocean-continent transition than to a slow-spreading ridge. Like in the Platta ocean-continent transition, basalts from other Alpine units once close to the rifted continental crust show T-MORB affinities (Gets nappe, Bill et al. 2000; external Ligurides, Vannucci et al. 1993; Balagne nappe, Venturelli et al. 1981), whereas more distal units contain N-MORB-type magmatic rocks (internal Ligurides, Venturelli et al. 1981, Vannucci et al. 1993, Rampone et al. 1998; Montgenèvre ophiolite, Venturelli et al. 1981; Inzecca, Venturelli et al. 1981). Isotopic data and geochemical modeling show that T-MORBs can be produced either by low degrees of melting of a depleted mantle source (external Liguride, Vannucci et al. 1993, Rampone et al.

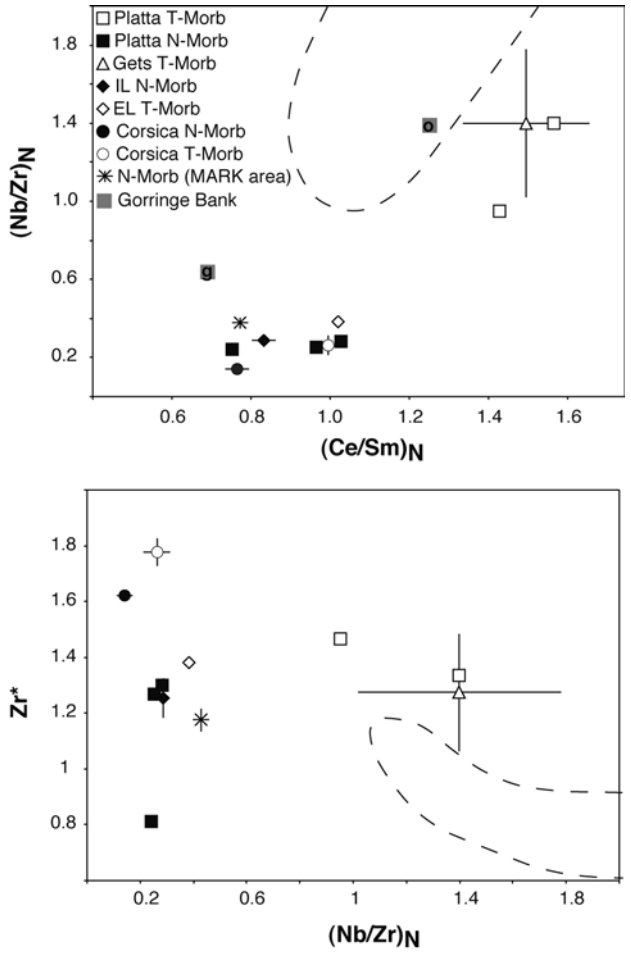

Fig. 11 **a** Incompatible-element ratio plots for T- and N-MORB of the Platta nappe and comparison with basalts from other Liguria-Piedmont ophiolites and from the Iberian margin. High Nb_n/Zr_n values for nappe of the Gets and Mt Ormonde (*o*) samples and Platta T-MORB indicate an enriched mantle source for these units whereas the lower values for the Platta N-MORBs, Ligurides, Corsica and Mt Gettysburg basalts (*g*) are similar to those of present-day N-MORBs. Note that the field of the Iberian abyssal plain basalts (*dashed line*) indicates more enriched sources. **b** Zr* ($Zr_n/((Sm_n + Nd_n)/2)$) vs. Nb_n/Zr_n plot. Zr* is sensitive to changes in the degree of partial melting producing the basalts whereas Nb_n/Zr_n is characteristic of the source of melting (see text for discussion). Data sources: nappe of the Gets, Bill et al. (2000); internal and external Ligurides, Rampone et al. (1998); Corsica, Saccani et al. (2000); Gorringe bank, Cornen et al. (1999); Iberia abyssal plain, Seifert et al. (1997) and Cornen et al. (1999); average N-MORB of the MARK area, Meurer et al. (2001)

1998) or by melting of a slightly enriched mantle probably of subcontinental origin (Bill et al. 2000). N-MORB shows limited compositional variation and is the product of moderate degrees of partial melting (< 10%) of a depleted mantle source (e.g., Vannucci et al. 1993). Our data show that the magmatic rock from the Platta ocean-continent transition record increasing degrees of melting and decreasing contamination of their source by an enriched component as they crystallized oceanwards. This process is probably related to the continuous thinning of the subcontinental mantle and the associated uplift of the underlying asthenosphere during progressive rifting and exhumation of subcontinental mantle between crustal and lithospheric breakup.

Conclusions

Within the Platta ocean-continent transition, the volume of mafic rocks, expressed by gabbros and basalts, increases oceanwards as most of the mafic rocks occur in the lower serpentinite unit.

The petrology and geochemistry of the gabbros shows that each continuous outcrop represents a different batch of melt which intruded the already exhumed and serpentinized mantle 161 Ma ago (Desmurs et al. 2001; Schaltegger et al. 2002). Each intrusion records different magmatic processes ranging from predominantly fractional crystallization to solidification without fractionation. The composition of the frozen melts as well as liquids calculated from the chemistry of the most primitive clinopyroxene cumulate indicates that the parental melt of the gabbros has the same range of composition as the overlying basalts.

Most of the basalts and the gabbro parental melts are already fractionated liquids in equilibrium with olivine cumulate and troctolite. These rock types were not found in the Platta nappe, which implies the occurrence of cumulate gabbros which can not be observed today.

The chemistry of the mafic liquids (basalts and parental melts of the gabbros) changes from T-MORB to N-MORB composition as they crystallized away from the continent. These rocks are the result of low degrees of melting of two distinct sources, a depleted (asthenospheric) mantle source for the N-MORBs and an 'enriched' mantle for the T-MORBs, which is probably the subcontinental mantle. We interpret the increasing degree of melting as the result of the upwelling asthenosphere after continental breakup during a transitional stage before the establishment of a slow-spreading system.

Acknowledgements Our work is part of the research project 'Comparative anatomy of passive continental margins: Iberia and Eastern Alps' supported by the Swiss National Science Foundation, projects 21-049117.96/1 and 20-55284.98. We thank U. Schaltegger, D. Bernoulli, Y. Lagabrielle, and F. Chalot-Prat for stimulating discussions and helpful suggestions. We are grateful to E. Reusser for technical assistance with the electron microprobe at the IMP of ETH Zürich, and to F. Chalot-Prat for help with the ICP-MS trace-element analysis performed at the CRPG, Nancy. Constructive reviews by J. Snow and G.B. Piccardo sharpened the presentation of this paper.

References

Bill M, Nägler TF, Masson H (2000) Geochemistry, Sm-Nd and Sr isotopes of mafic rocks from the earliest oceanic crust of Alpine Tethys. Schweiz Mineral Petrogr Mitt 80:131–145

Boillot G, Recq M, Winterer EL, Meyer AW, Applegate J, Baltuck M, Bergen JA, Comas MC, Davies TA, Dunham K, Evans CA, Girardeau J, Goldberg G, Haggerty J, Jansa LF, Johnson JA,

Loreau J, Kasahara JP, Luna-Sierra E, Moullade M, Ogg J, Sarti M, Thurow J, Williamson M (1987) Tectonic denudation of the upper mantle along passive margin: a model based on drilling results (ODP Leg 103, Western Galicia Margin, Spain). Tectonophysics 132:334–342

Casey JF (1997) Comparison of major- and trace-element geochemistry of abyssal peridotites and mafic plutonic rocks with basalts from the MARK region of the Mid-Atlantic Ridge. Proc Ocean Drill Program Sci Res 153:181–241

Charpentier S, Kornprobst J, Chazot G, Cornen G, Boillot G (1998) Interaction entre lithosphère et asthenosphère au cours de l'ouverture océanique: données isotopiques préliminaires sur la Marge passive de Galice (Atlantique-Nord). C R Acad Sci Paris 326:757–762

Christie DM, Carmichael ISE, Langmuir CH (1986) Oxidation states of mid-ocean ridge basalt glasses. Earth Planet Sci Lett 79:397–411

Cornelius HP (1932) Geologische Karte der Err-Julier Gruppe 1:25'000. Schweiz Geol Komm Spezialkarte nr 115A

Cornen G, Girardeau J, Monnier C (1999) Basalts, underplated gabbros and pyroxenites record the rifting process of the West Iberian margin. Mineral Petrol 67:111–142

Desmurs L, Manatschal G, Bernoulli D (2001) The Steinmann trinity revisited: mantle exhumation and magmatism along an ocean-continent transition: the Platta nappe, eastern Switzerland. In: Wilson RCL, Whitmarsh RB, Taylor B, Froitzheim N (eds) Non-volcanic rifting of continental margins: a comparison of evidence from land and sea. Geol Soc Lond Spec Publ 187:235–266

Dick HJB, Natland JH, Alt JC et al. (2000) A long in situ section of the lower ocean crust: results of ODP Leg 176 drilling at the Southwest Indian Ridge. Earth Planet Sci Lett 179:31–51

Dietrich V (1969) Die Ophiolithe des Oberhalbsteins (Graubünden) und das Ophiolithmaterial der ostschweizerischen Molasseablagerungen, ein petrographischer Vergleich. Herbert Lang, Bern

Ferreiro-Mählmann R (1995) Das Diagenese-Metamorphose-Muster von Vitrinit-Reflexion und Illit-"Kristallinität" in Mittelbünden und im Oberhalbstein, Teil 1: Bezüge zur Stockwerktektonik. Schweiz Mineral Petrogr Mitt 75:85–122

Frisch W, Ring U, Dürr S, Borchert S, Biehler D (1994) The Arosa zone and Platta nappe ophiolites (Eastern Swiss Alps): Geochemical characteristics and their meaning for the evolution of the Penninic Ocean. Jahrb Geol Bundesanst Wien 137:19–33

Froitzheim N, Eberli GP (1990) Extensional detachment faulting in the evolution of a Tethys passive continental margin (Eastern Alps, Switzerland). Geol Soc Am Bull 102:1297–1308

Froitzheim N, Manatschal G (1996) Kinematics of Jurassic rifting, mantle exhumation, and passive-margin formation in the Austroalpine and Penninic nappes (eastern Switzerland). Geol Soc Am Bull 108:1120–1133

Froitzheim N, Schmid SM, Conti P (1994) Repeated change from crustal shortening to orogen-parallel extension in the Austroalpine units of Graubünden. Eclogae Geol Helv 87:559–612

Froitzheim N, Schmid SM, Frey M (1996) Mesozoic paleogeography and the timing of eclogite-facies metamorphism in the Alps: A working hypothesis. Eclogae Geol Helv 89:81–110

Grove TL, Kinzler RJ, Brian WB (1992) Fractionation of mid-ocean ridge basalts (MORB). In: Morgan JP et al. (eds) Mantle flow and melt generation at mid-ocean ridges. Geophys Monogr Ser AGU, Washington, DC, pp 281–310

Hart SR, Dunn T (1993) Experimental Cpx/melt partitioning of 24 trace elements. Contrib Mineral Petrol 113:1–8

Karson JA, Lawrence RM (1997) Tectonic window into gabbroic rocks of the middle oceanic crust in the MARK area near site 921–924. Proc Ocean Drill Program Sci Res 153:181–241

Kinzler RJ, Grove TL, Recca SI (1990) An experimental study of temperature and melt composition on the partitioning of nickel between olivine and silicate melt. Geochim Cosmochim Acta 54:1255–1265

Kornprobst J, Vidal P, Malod J (1988) Les basaltes de la marge de Galice (nord-ouest de la péninsule ibérique) : hétérogénéité des spectres des terres rares à la transition continent-océan. Données géochimiques préliminaires. C R Acad Sci Paris 306:1359–1364

Lagabrielle Y, Lemoine M (1997) Alpine Corsican and Apennine ophiolites: the slow-spreading ridge model. C R Acad Sci Paris 325:909–920

Langmuir CH (1989) Geochemical consequences of in situ crystallization. Nature 340:199–205

Lemoine M, Tricart P, Boillot G (1987) Ultramafic and gabbroic ocean floor of the Ligurian Tethys (Alps, Corsica, Apennines): In search of a genetic model. Geology 15:622–625

Manatschal G, Nievergelt P (1997) A continent-ocean transition recorded in the Err and Platta nappes (eastern Switzerland). Eclogae Geol Helv 90:3–27

Meurer WP, Sturm MA, Klein EM, Karson JA (2001) Basalt compositions from the Mid-Atlantic ridge at the SMARK area (22°30′ to 22°50′) – implications for parental liquid variability at isotopically homogeneous spreading centers. Earth Planet Sci Lett 186:451–469

Müntener O, Hermann J (1996) The Val Malenco lower crust – upper mantle complex and its field relations (Italian Alps). Schweiz Mineral Petrogr Mitt 76:475–500

Müntener O, Hermann J (2001) The role of lower crust and continental upper mantle during formation of nonvolcanic passive continental margins: evidence from the Alps. In: Wilson RCL, Whitmarsh RB, Taylor B, Froitzheim N (eds) Non-volcanic rifting of continental margins: a comparison of evidence from land and sea. Geol Soc Lond Spec Publ 187:267–288

Müntener O, Hermann J, Trommsdorff V (2000) Cooling history and exhumation of lower-crustal granulite and upper mantle (Malenco, Central Alps). J Petrol 41:1–25

Piccardo GB, Rampone E, Vannucci R (1990) Upper mantle evolution during continental rifting and ocean formation; evidences from peridotite bodies of the Western Alpine-Northern Apennine system. In: Roure F, Heitzmann P, Polino R (eds) Deep structure of the Alps. Mém Soc Géol Fr 156:323–333

Puschnig AR (2000) The oceanic Forno Unit (Rhetic Alps). Eclogae Geol Helv 93:103–124

Rampone E, Hofmann AW, Piccardo GB, Vannucci R, Bottazzi P, Ottolini L (1995) Petrology, mineral and isotope geochemistry of the external Liguride peridotites (northern Apennines, Italy). J Petrol 36:81–105

Rampone E, Hofmann AW, Raczek (1998) Isotopic contrasts within the Internal Liguride Ophiolite (N. Italy): the lack of a genetic mantle-crust link. Earth Planet Sci Lett 163:175–189

Roeder PL, Emslie RF (1970) Olivine-liquid equilibrium. Contrib Mineral Petrol 29:275–289

Saccani E, Padoa E, Tassinari R (2000) Preliminary data on the Pineto gabbroic massif and Nebbio basalts: Progress toward the geochemical characterization of Alpine Corsica ophiolites. Ofioliti 25:75–85

Schaltegger U, Desmurs L, Manatschal G, Müntener O, Meier M, Bernoulli D (2002) Transition from a rifted continental margin to a slow spreading system: field and isotopic constraints from a Tethyan ophiolite. Terra Nova 14:156–162

Schärer U, Kornprobst J, Beslier MO, Boillot G, Girardeau J (1995) Gabbro and related rock emplacement beneath rifting continental crust: U-Pb geochronological and geochemical constraints for the Galicia passive margin (Spain). Earth Planet Sci Lett 130:187–200

Schärer U, Girardeau J, Cornen G, Boillot G (2000) 138–121 Ma asthenospheric magmatism prior to continental break-up in the North Atlantic and geodynamic implications. Earth Planet Sci Lett 181:555–572

Seifert KE, Chang C-W, Brunotte DA (1997) Evidence from Ocean Drilling Program Leg 149 mafic igneous rock for oceanic crust in the Iberia Abyssal Plain ocean-continent zone. J Geophys Res 102:7915–7928

Stille P, Clauer N, Abrecht J (1989) Nd isotopic composition of Jurassic seawater and the genesis of Alpine Mn deposits: evidence from Sr-Nd isotope data. Geochim Cosmochim Acta 53:1095–1099

Sun SS, McDonough WF (1989) Chemical and isotopic systematics of oceanic basalts: implication for mantle composition and processes. In: Saunders AD, Norry MJ (eds) Magmatism in the ocean basins. Geol Soc Lond Spec Publ 42:313–345

Tiepolo M, Tribuzio R, Vannucci R (1997) Mg- and Fe-gabbroids from Northern Apennine ophiolites: Parental liquids and differentiation process. Ofioliti 22:57–69

Tribuzio R, Tiepolo M, Vannucci R, Bottazzi P (1999) Trace element distribution within olivine-bearing gabbros from the Northern Apennine ophiolites (Italy): evidence for post-cumulus crystallization in MOR-type gabbroic rocks. Contrib Mineral Petrol 134:123–133

Trommsdorff V (1983) Metamorphose magnesiumreicher Gesteine: Kritischer Vergleich von Natur, Experiment und thermodynamischer Datenbasis. Fortschr Mineral 61:283–308

Trommsdorff V, Evans B (1974) Alpine metamorphism of peridotitic rocks. Schweiz Mineral Petrogr Mitt 54:333–352

Trommsdorff V, Piccardo GB, Montrasio A (1993) From magmatism through metamorphism to sea floor emplacement of subcontinental Adria during pre-Alpine rifting (Malenco, Italy). Schweiz Mineral Petrogr Mitt 73:191–203

Ulmer P (1989) The dependence of the Fe^{2+}-Mg cation-partitioning between olivine and basaltic liquid on pressure, temperature and composition; an experimental study to 30 kbars. Contrib Mineral Petrol 101:261–273

Vannucci R, Rampone E, Piccardo GB, Ottolini L, Bottazzi P (1993) Ophiolitic magmatism in the Ligurian Tethys; an ion microprobe study of basaltic clinopyroxenes. Contrib Mineral Petrol 115:123–137

Venturelli G, Thorpe RS, Potts PJ (1981) Rare earth and trace element characteristics of ophiolitic metabasalts from the Alpine-Apennine belt. Earth Planet Sci Lett 53:109–123

Whitmarsh RB, Minshull TA, Russel SM, Dean SM, Louden KE, Chian D (2001) The role of syn-rift magmatism in the rift-to-drift evolution of the west Iberia margin: geophysical observations. In: Wilson RCL, Whitmarsh RB, Taylor B, Froitzheim N (eds) Non-volcanic rifting of continental margins: a comparison of evidence from land and sea. Geol Soc Lond Spec Publ 187:107–124